Article
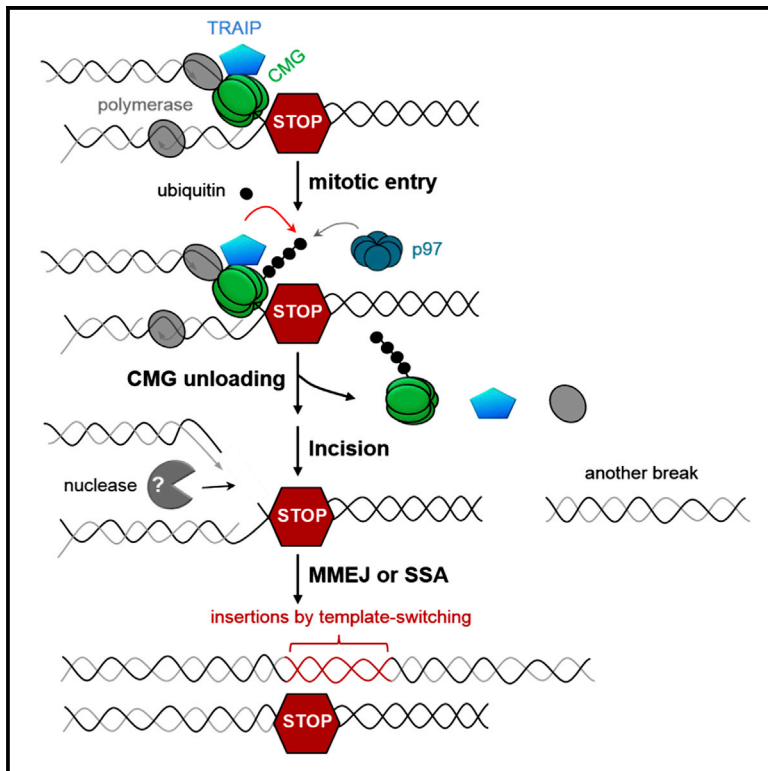
Mitotic CDK Promotes Replisome Disassembly, Fork Breakage, and Complex DNA Rearrangements

Graphical Abstract

Authors

Lin Deng, R. Alex Wu, Remi Sonneville, Olga V. Kochenova, Karim Labib, David Pellman, Johannes C. Walter

Correspondence

david_pellman@dfci.harvard.edu (D.P.), johannes_walter@hms.harvard.edu (J.C.W.)

In Brief

Mitotic entry before completion of DNA replication causes genome instability via an unknown mechanism. Using *Xenopus* egg extracts, Deng et al. find that mitotic cyclin-dependent kinase triggers replication fork breakage and DNA rearrangements. The mechanism requires TRAIP-dependent ubiquitylation of the replicative helicase followed by p97 ATPase-dependent helicase removal from chromatin.

Highlights

- Replication fork collapse is triggered by mitotic CDK-dependent CMG unloading

- Mitotic CMG unloading requires the E3 ubiquitin ligase TRAIP and the p97 ATPase

- Mitotic processing of stalled forks enables high-fidelity chromosome segregation

- New model for the generation of complex chromosome rearrangements

CellPress

Mitotic CDK Promotes Replisome Disassembly, Fork Breakage, and Complex DNA Rearrangements

Lin Deng,[1,2,3] R. Alex Wu,[3] Remi Sonneville,[4] Olga V. Kochenova,[3] Karim Labib,[4] David Pellman,[1,2,5,6,7,*] and Johannes C. Walter[3,6,7,8,*]

[1]Department of Pediatric Oncology, Dana-Farber Cancer Institute, Boston, MA 02215, USA
[2]Department of Cell Biology, Harvard Medical School, Blavatnik Institute, Boston, MA 02115, USA
[3]Department of Biological Chemistry and Molecular Pharmacology, Harvard Medical School, Blavatnik Institute, Boston, MA 02115, USA
[4]MRC Protein Phosphorylation and Ubiquitylation Unit, Sir James Black Centre, School of Life Sciences, University of Dundee, Dow Street, Dundee DD1 5EH, UK
[5]Broad Institute of MIT and Harvard, Cambridge, MA 02142, USA
[6]Howard Hughes Medical Institute, Boston, MA 02115, USA
[7]These authors contributed equally
[8]Lead Contact
*Correspondence: david_pellman@dfci.harvard.edu (D.P.), johannes_walter@hms.harvard.edu (J.C.W.)
https://doi.org/10.1016/j.molcel.2018.12.021

SUMMARY

DNA replication errors generate complex chromosomal rearrangements and thereby contribute to tumorigenesis and other human diseases. One mechanism that triggers these errors is mitotic entry before the completion of DNA replication. To address how mitosis might affect DNA replication, we used *Xenopus* egg extracts. When mitotic CDK (Cyclin B1-CDK1) is used to drive interphase egg extracts into a mitotic state, the replicative CMG (CDC45/MCM2-7/GINS) helicase undergoes ubiquitylation on its MCM7 subunit, dependent on the E3 ubiquitin ligase TRAIP. Whether replisomes have stalled or undergone termination, CMG ubiquitylation is followed by its extraction from chromatin by the CDC48/p97 ATPase. TRAIP-dependent CMG unloading during mitosis is also seen in *C. elegans* early embryos. At stalled forks, CMG removal results in fork breakage and end joining events involving deletions and templated insertions. Our results identify a mitotic pathway of global replisome disassembly that can trigger replication fork collapse and DNA rearrangements.

INTRODUCTION

Genome evolution occurs through the gradual accrual of genetic changes or in a saltatory manner, with bursts of chromosomal alterations originating from single catastrophic events (Holland and Cleveland, 2012; Leibowitz et al., 2015; Liu et al., 2011; Stephens et al., 2011). Many chromosomal alterations can be traced to DNA breaks that arise during DNA replication (Hills and Diffley, 2014; Mankouri et al., 2013; Técher et al., 2017). However, when and how replication fork breakage is triggered remains incompletely understood (Toledo et al., 2017).

In normal cells, multiple cell cycle-regulatory controls and error correction mechanisms prevent DNA replication errors (Hills and Diffley, 2014). Cells prepare for DNA replication in the G1 phase of the cell cycle, when pairs of MCM2-7 ATPases are recruited to each origin ("licensing"). In S phase, cyclin-dependent kinase (CDK) promotes the association of CDC45 and GINS with MCM2-7, leading to formation of the replicative CMG helicase complex (CDC45-MCM2-7-GINS) ("initiation"). CMG unwinding of the origin nucleates the assembly of two DNA replication forks that travel away from the origin, copying DNA as they go ("elongation"). When converging forks from adjacent origins meet, the replisome is disassembled ("termination"). Replisome disassembly in metazoans requires the E3 ubiquitin ligase CRL2[Lrr1], which ubiquitylates the MCM7 subunit of CMG, leading to CMG's extraction from chromatin by the p97 ATPase (Dewar et al., 2017; Sonneville et al., 2017). In the absence of CRL2[Lrr1], CMGs persist on chromatin until mitosis but are then removed by a secondary, p97-dependent pathway that is controlled by an unknown E3 ubiquitin ligase (Sonneville et al., 2017). Re-replication is inhibited because *de novo* licensing of origins is suppressed in the S and G2 phases of the cell cycle. Thus, faithful DNA replication requires the seamless integration of replication licensing, initiation, elongation, and termination. Errors in the process are detected by the DNA damage response, which activates repair mechanisms and prevents entry into mitosis in the setting of incomplete or abnormal replication.

DNA replication forks become stressed in a variety of circumstances, including the activation of oncogenes, collision with DNA lesions and other obstacles, and nucleotide starvation (Cortez, 2015; Hills and Diffley, 2014; Saldivar et al., 2017). Replication stress can cause replication fork "collapse," an irreversible state from which replication does not restart (Cortez, 2015; Hills and Diffley, 2014; Pasero and Vindigni, 2017; Saldivar et al., 2017; Toledo et al., 2017). Numerous experiments suggested that fork collapse involves replisome disassembly (Cortez, 2015). However, these studies did not establish a causal relationship between replisome disassembly and collapse, and other studies have concluded that fork collapse may not involve

replisome disassembly (De Piccoli et al., 2012; Dungrawala et al., 2015). Fork collapse is frequently associated with MUS81-dependent breakage of DNA strands at the fork (Pasero and Vindigni, 2017), but whether collapse and breakage are mechanistically distinct phenomena remains unclear.

Although replication fork breakage is generally viewed as a source of gross chromosomal rearrangements, breakage may sometimes preserve genome integrity (Bhowmick and Hickson, 2017). A well-studied example involves common fragile sites (CFSs), which are among the most frequently rearranged genomic loci in cancer genomes (Glover et al., 2017). Common fragile site "expression," the appearance of cytologically visible breaks and gaps, is promoted by low doses of aphidicolin, which delays duplication of these already late-replicating loci. Unreplicated DNA at CFSs forms ultrafine DNA bridges between anaphase chromosomes (Baumann et al., 2007; Chan et al., 2007), and severance of these bridges by MUS81 is thought to allow chromosome segregation. However, random breakage of the fork would yield deleterious outcomes, such as the generation of acentric or iso-chromosomes. So far, no mechanism has emerged that explains whether and how such outcomes can be avoided.

Although breakage of a few stressed forks may be beneficial, concurrent breakage of many forks generates catastrophic chromosomal rearrangements. Several lines of evidence implicate mitotic entry with unreplicated DNA as one potential cause of extensive fork breakage. Cell fusion experiments (Johnson and Rao, 1970) and experiments on cells with micronuclei (Kato and Sandberg, 1968) showed that S phase chromosomes undergo "pulverization" upon exposure to mitotic cytoplasm. Although there was early disagreement about whether chromosome pulverization reflects discontinuous condensation or DNA breakage (Rao et al., 1982), current work indicates that chromosome pulverization usually reflects DNA fragmentation. First, premature mitotic entry triggered by inhibition of the WEE1 kinase causes extensive fork breakage that depends on the formation of an active MUS81 complex (Domínguez-Kelly et al., 2011; Duda et al., 2016). Second, chromothripsis, a mutational process involving extensive chromosome fragmentation and rearrangement, may involve entry into mitosis of micronuclei undergoing DNA replication (Crasta et al., 2012; Leibowitz et al., 2015). Extensive fork breakage during mitosis is especially problematic because both homologous recombination (HR) and classical non-homologous end joining (NHEJ) are suppressed at this stage of the cell cycle (Hustedt and Durocher, 2016). In summary, it has become apparent that genome instability in a variety of contexts is linked to mitotic replication fork breakage. However, why forks are so fragile in mitosis is unclear.

Here we use *Xenopus* egg extracts to explore the relationship between DNA replication and mitosis. We find that, in extracts supplemented with the mitotic kinase Cyclin B1-CDK1, the RING E3 ubiquitin ligase TRAIP is required for the ubiquitylation of CMG helicase at stalled and terminated forks. Ubiquitylated CMG is extracted from chromatin by the CDC48 or p97 ATPase. At stalled forks, CMG unloading leads to fork breakage and end joining events that appear to depend on DNA polymerase θ (Polθ). Unlike Cyclin B1-CDK1 treatment, ATR inhibition does not lead to breakage of stalled forks. Together, our results identify TRAIP-dependent replisome disassembly as a crucial step in mitotic replication fork collapse and breakage. We propose that the effect of TRAIP-induced fork breakage on genome stability depends on how many forks are present when cells enter mitosis.

RESULTS

Mitotic CDK Triggers Aberrant Processing of Stressed DNA Replication Forks

To examine the effect of mitotic CDK on DNA replication and fork stability, we used *Xenopus* egg extracts, which can recapitulate S phase or mitosis. For S phase, plasmid DNA was first incubated in a high-speed supernatant (HSS) of *Xenopus* egg extract. HSS promotes the assembly onto DNA of pre-replication complexes (pre-RCs) containing double hexamers of the MCM2-7 ATPase (Figure 1A). The subsequent addition of a nucleoplasmic extract (NPE) leads to the association of CDC45 and GINS with each MCM2-7 hexamer to form two active CMG DNA helicases that unwind DNA, promoting a single, complete round of DNA replication, manifested as the appearance of supercoil (SC) daughter molecules (Figure 1B, lanes 1–6; Walter et al., 1998). To achieve replication in a mitotic state, we added Cyclin B1-CDK1 (B1-CDK1) after licensing and before NPE addition because this kinase inhibits licensing (Hendrickson et al., 1996; Prokhorova et al., 2003; Figure 1A). We confirmed that, in this sequence, B1-CDK1 induced chromosome condensation (Figures S1A–S1C) and condensin recruitment (Figures S1D and S1E). As we showed previously (Prokhorova et al., 2003), B1-CDK1 increased the rate of DNA replication (Figure 1B, compare lanes 1–6 and 13–18), in part because of increased origin firing (Figure S1F). However, in the absence of other perturbations, all replication products comprised open circular or supercoiled species (Figure 1B, lanes 13–18), indicating that B1-CDK1-induced chromatin condensation does not cause aberrant DNA replication.

Given that stressed DNA replication forks appear to undergo breakage during mitosis, we added a low concentration of the replicative DNA polymerase inhibitor aphidicolin (APH) to slow fork progression (Figure 1B, lanes 7–12). The combination of B1-CDK1 and APH led to the appearance of a new replication product that migrated at the very top of the gel (Figure 1B, lane 24). This aberrant replication product (ARP) comprised ~6% of total replication for a 3-kb plasmid and up to 30% for a 9-kb plasmid (data not shown), presumably because the larger plasmid hosts more replication forks. ARPs recovered from extract were not resolved by Topoisomerase I or Topoisomerase II, indicating that they are not plasmid topoisomers (data not shown). Thus, in the presence of replication stress, mitotic CDK induces aberrant DNA replication.

To examine the effect of B1-CDK1 on replication forks that have stalled at a defined location, we replicated a plasmid containing an array of 48 *lacO* sites (p[*lacO*₄₈]) bound by the *lac* repressor (LacR) (Figure 1C). As expected (Dewar et al., 2015), replication forks accumulated at the outer edges of the LacR array, generating a "theta" (θ) structure (Figures 1C and 1D, lanes 11–15). In the presence of B1-CDK1, the theta molecules disappeared, and ARPs accumulated (Figure 1D, lanes 16–20). ARPs were not generated when LacR-mediated fork stalling
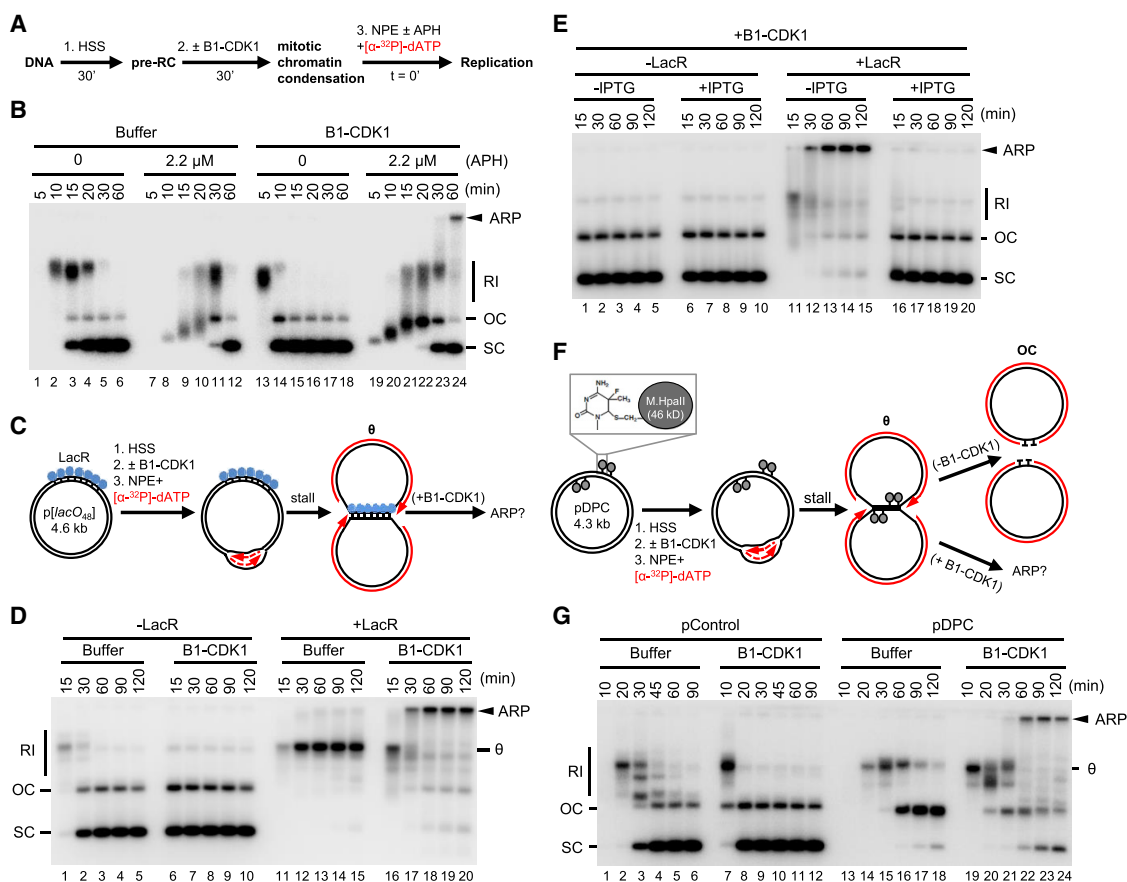
Figure 1. Mitotic CDK Triggers Aberrant Processing of Stalled DNA Replication Forks in *Xenopus* Egg Extracts

(A) Schematic of the experimental approach to test the effect of B1-CDK1 on DNA replication. APH, aphidicolin.

(B) A 3-kb pBlueScript plasmid was replicated according to (A), and products were separated on a native agarose gel followed by autoradiography. Unless stated otherwise, the 0 minute time point refers to NPE addition.

(C) Schematic of DNA replication for the LacR-bound p[*lacO*48] plasmid.

(D) p[*lacO*48] was replicated according to (C) under the indicated conditions.

(E) p[*lacO*48] was replicated according to (C) in the absence or presence of LacR and IPTG (10 mM, 15 min incubation in NPE before mixing with the licensing mixture), as indicated.

(F) Schematic of replication for pDPC, containing four 46-kDa M.HpaII DNA methyltransferases at the indicated positions. Products formed in the presence and absence of B1-CDK1 are indicated.

(G) pControl or pDPC was replicated according to (F) using the indicated conditions.

From (A) to (G), B1-CDK1 was added to the licensing mixture at a concentration of 50 ng/μL, and its final concentration in the overall reaction was 16.7 ng/μL (STAR Methods). RI, replication intermediate; OC, open circle; SC, supercoil; θ, theta structure; ARP, aberrant replication product. See also Figure S1.

was prevented with isopropyl β-D-1-thiogalactopyranoside (IPTG) (Figure 1E) or in the presence of the CDK1 inhibitor (CDK1-i) RO-3306 (Figure S1G). Furthermore, addition of Cyclin E-CDK2 or Cyclin A2 (which preferentially associates with endogenous CDK1; Strausfeld et al., 1996) did not induce ARPs, although their addition accelerated DNA replication, as expected (Figure S1H). Second, we replicated a plasmid substrate (pDPC) that contains two site-specific DNA-protein cross-links (DPCs) on each leading strand template (Figure 1F). As expected (Duxin et al., 2014), in the absence of B1-CDK1, replication of pDPC first yielded theta structures when forks transiently paused at the DPC. Plasmids then resolved into open circle (OC) species that persisted because of slow translesion synthesis past the peptide adduct generated by DPC proteolysis

(Figure 1F, top arrow, and Figure 1G, lanes 13–18). In the presence of B1-CDK1, we again observed abundant ARPs (Figure 1G, lanes 19–24). In summary, mitotic CDK caused aberrant processing of replication forks stalled by APH, non-covalent nucleoprotein complexes, and DPCs.

Mitotic Processing of Stalled Replication Forks Leads to Complex Chromosomal Rearrangements

To determine the structure of mitotic ARPs, we replicated the 4.6-kb LacR plasmid in the presence and absence of B1-CDK1 and digested the replication products with AlwNI and AflII, which cuts the plasmid into a 1.9-kb fragment and a 2.7-kb fragment encompassing the *lacO* repeats (Figure 2A). In the absence of B1-CDK1, fully replicated 1.9-kb fragments quickly accumulated,
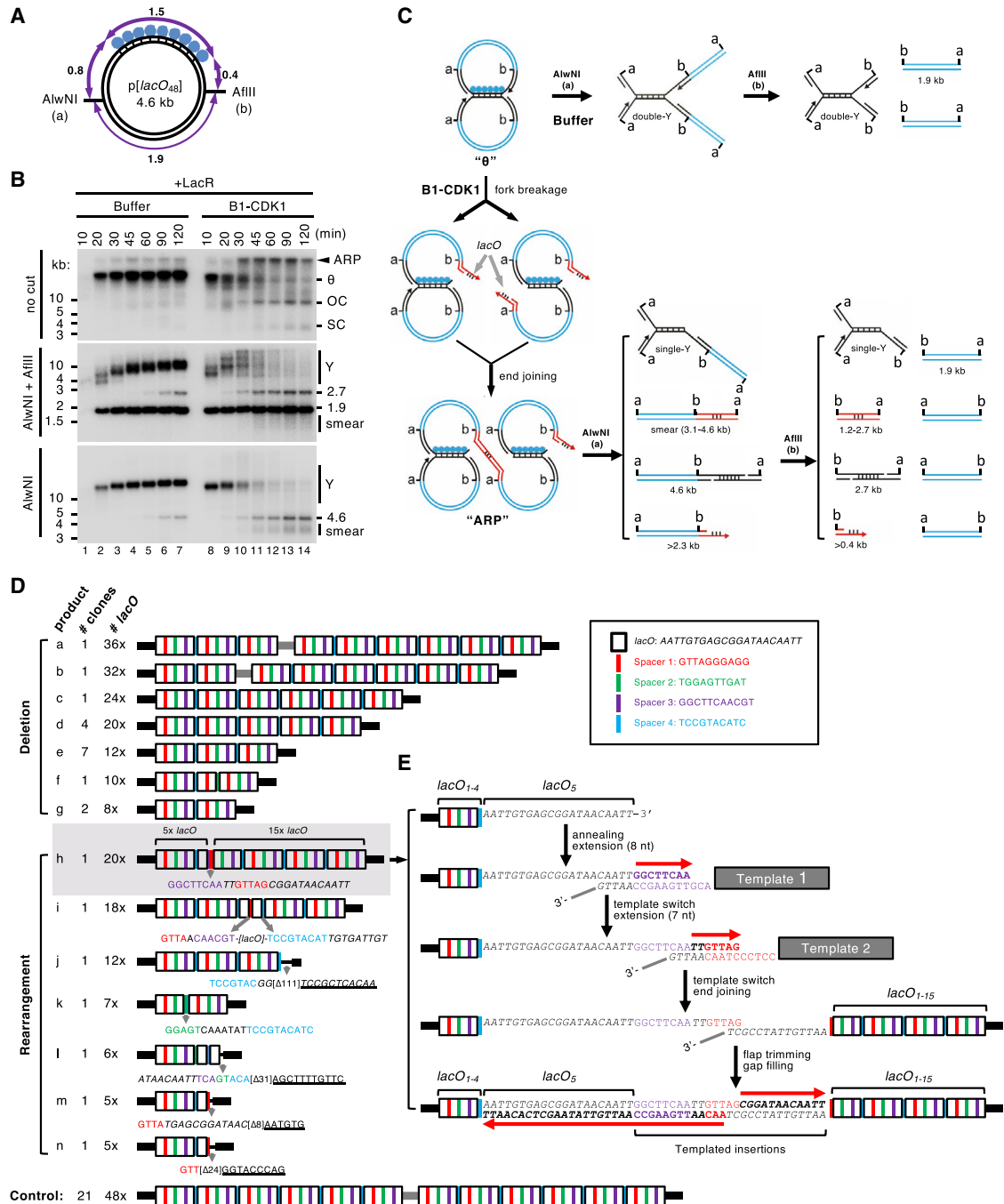
Figure 2. Mitotic Processing of Stalled Replication Forks Leads to Complex DNA Rearrangements

(A) Structure of the 4.6-kb p[lacO₄₈] plasmid. Numbers mark the length of the indicated DNA segments in kilobase pairs.

(B) p[lacO₄₈] was replicated in the presence of buffer or B1-CDK1. At the indicated time points, replication products were isolated and digested with AlwNI and AflII or AlwNI as indicated. Numbers label the size of linear fragments in kilobase pairs. Y, double-Y or single-Y structure (see C).

(C) Model explaining the restriction products observed in (B). Although the model favors fork breakage on the leading strand, the possibility of fork breakage on the lagging strand has not been excluded. A more detailed model is presented in Figure S2A.

(D) The smear of ∼3- to 4-kb mitotic DNA replication products generated after AlwNI digestion in (B) was self-ligated, cloned, and sequenced. The controls are replication products of the same plasmid from a mitotic reaction lacking LacR. The lacO repeats, shown as white boxes, are separated by four unique spacers shown in different colors. Inset, DNA sequences of the lacO repeat and four spacers. The detailed structure of the entire lacO array is shown in Figure S2C.

(E) A model for the generation of product h in (D) from multiple template-switching events.

See also Figure S2.

whereas the rest of the plasmid migrated as a double-Y structure that gradually increased in size because of slow progression of forks through the LacR array (Figure 2B, center, lanes 1–7, and Figure 2C, Buffer; Dewar et al., 2015). In the presence of B1-CDK1, the 1.9-kb fragment again accumulated quickly and persisted, demonstrating that this *lacO*-free region was replicated efficiently (Figure 2B, center, lanes 8–14). However, the double-Y structure containing the *lacO* array rapidly disappeared. Thus, in the presence of B1-CDK1, aberrant DNA processing occurs specifically on molecules containing stalled forks.

When the replication products were digested only with AlwNI, we observed B1-CDK1-dependent disappearance of the now larger double-Y structure (Figure 2B, bottom, lanes 8–14). In addition, we detected a new series of species migrating between ∼3 and ∼4 kb (Figure 2B, bottom, smear). We hypothesized that, when replication forks enter the array and slow down or stall, B1-CDK1 promotes their collapse and breakage. The resulting double-strand breaks (DSBs) subsequently undergo joining with DSBs from broken forks on other plasmids, generating ARPs (Figures 2C, B1-CDK1, and S2A). If replication forks collapse at the outer edges of the array, then the size of the end joining product after AlwNI digestion is close to 3.1 kb because most of the 1.5-kb *lacO* array is lost; collapse further into to the array generates larger products, accounting for the 3- to 4-kb range of products observed (Figure S2B). To test this hypothesis, the 3- to 4-kb species were cloned and sequenced using primers immediately flanking the *lacO* array (Figure S2C). In contrast to control clones (generated from replication in the absence of LacR), all of which contained 48 *lacO* repeats, the 24 clones from the 3- to 4-kb smear contained fewer than 48 *lacO* repeats (Figure 2D, products a–n). This result confirms that replication forks collapsed within the *lacO* array and then underwent end joining with loss of *lacO* repeats. Seventeen of these products (a–g) involved only deletions of the *lacO* repeats. This suggests that the deletions might occur via single-strand annealing (SSA) (Bhargava et al., 2016), which generates deletions between homologous sequences. The remaining 7 clones contained complex rearrangements with microhomology at the junction or insertions that likely arose from replication template-switching events (Figure 2D, products h–n). For example, product h appears to have arisen from fork collapse at the fifth repeat, followed by two successive microhomology-mediated strand invasion and copying events, followed by joining to a second fork that broke at the 15th repeat (Figure 2E). The sequencing data strongly suggest that stressed replication forks collapse in the presence of B1-CDK1, generating DSBs that subsequently undergo end joining, sometimes after repeated template-switching.

Immunodepletion of DNA Polθ Reduces Mitotic ARPs

We next addressed the mechanism of end joining after B1-CDK1-induced fork collapse. As expected (Peterson et al., 2011), RAD51, which is essential for HR, did not bind chromatin in the presence of B1-CDK1 (Figure S3A), and inhibition of RAD51 function in extracts had no effect on B1-CDK1-induced ARP formation (Figures S3B–S3D). Further, classical NHEJ was not required for ARP formation (Figure S3E). The structures of the mitotic ARPs (Figures 2C–2E) suggested that MMEJ (microhomology-

mediated end joining, also called alternative end joining) is responsible for some mitotic DSB repair. Indeed, immunodepletion of Polθ (Figure 3A), a major mediator of MMEJ known to undergo template-switching (Wyatt et al., 2016), decreased ARPs during replication of LacR plasmid (Figures 3B and S3F) and pDPC (Figures 3C and S3G). Additionally, Polθ depletion resulted in overall lower amounts of replication products (Figures S3F and S3G), probably because of resection of unligated nascent strands. Finally, Polθ depletion virtually eliminated ARPs containing complex rearrangements (Figures 3D and 3E). Thus, in mitotic extracts where HR and NHEJ are inactive, MMEJ appears to play an important role in joining DNA ends after fork breakage.

Condensin Is Dispensable for Mitotic CDK-Induced Fork Instability

Mitotic chromatin condensation has long been proposed to cause DNA damage in under-replicated regions (El Achkar et al., 2005; Lukas et al., 2011). We therefore investigated the role of chromatin condensation on fork collapse in mitotic egg extracts. Although immunodepletion of the condensin subunit SMC2 inhibited B1-CDK1-induced chromosome condensation (Figures S4A and S4B), it did not affect the formation of ARPs (Figures S4C and S4D). Therefore, chromatin condensation per se is neither necessary nor sufficient for fork instability in mitotic egg extracts.

CMG Unloading at Stalled Forks Initiates Mitotic Fork Breakage

When two replication forks converge on a DNA inter-strand crosslink (ICL) in interphase egg extracts, CMG ubiquitylation and unloading from chromatin by the CDC48 or p97 ATPase leads to DNA incisions that generate a double-stranded DNA break (Amunugama et al., 2018; Fullbright et al., 2016; Klein Douwel et al., 2014; Semlow et al., 2016). We therefore asked whether B1-CDK1-induced fork breakage at single stalled forks is caused by CMG unloading. As shown previously (Dewar et al., 2015), CMGs that stalled at a LacR array did not dissociate from chromatin in interphase extracts (Figure 4A, lane 1). In contrast, in the presence of B1-CDK1, CMGs were unloaded (Figure 4A, lane 5). Addition of the p97 inhibitor NMS-873 (p97-i) prevented B1-CDK1-triggered CMG unloading and revealed a ladder of MCM7 species (Figure 4A, lane 7, red bracket) that was collapsed by USP21, a non-specific deubiquitylating enzyme (Figure 4A, lane 8). Therefore, B1-CDK1 induces MCM7 ubiquitylation and p97-dependent CMG unloading at single stalled forks, demonstrating that, under mitotic conditions, fork convergence is not required for CMG unloading. Strikingly, p97-i suppressed the formation of ARPs on the LacR plasmid (Figure 4B), suggesting that fork breakage requires CMG unloading. Consistent with this interpretation, CMG unloading normally preceded replication fork breakage (Figure S4E). Interestingly, in the presence of p97-i, theta structures were converted to mature replication products (OC and SC) more efficiently in the presence of B1-CDK1 than in its absence (Figure 4B, compare lanes 16–20 and 6–10), suggesting that B1-CDK1 may promote fork progression through the array when CMG unloading is prevented. Treatment with p97-i also reduced the mitotic CDK-induced H2AX
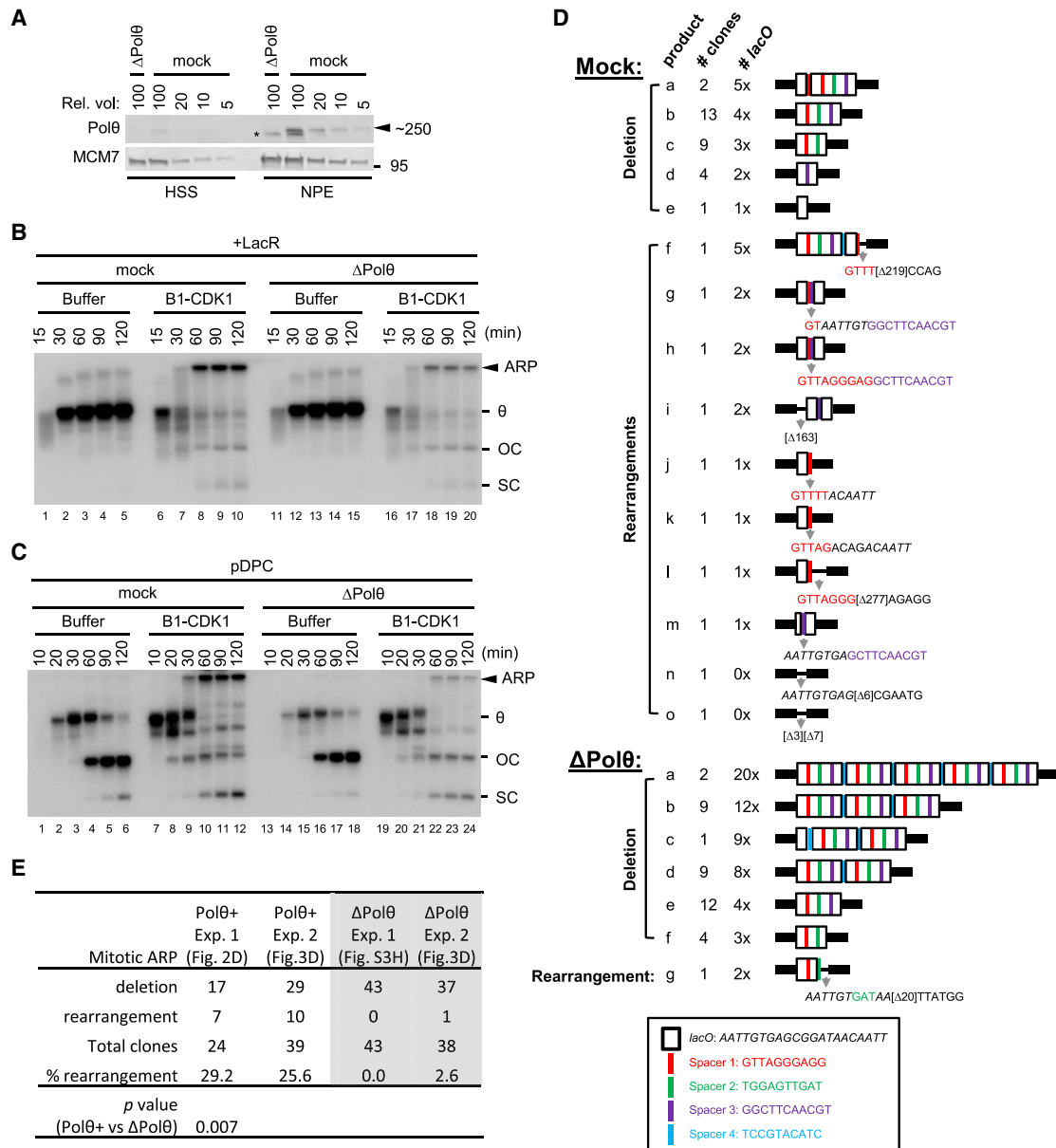
Figure 3. Depletion of DNA Polymerase θ Disrupts the Generation of Aberrant Replication Products in the Presence of Mitotic CDK

(A) Mock-depleted and DNA polymerase θ (Polθ-depleted *Xenopus* egg extracts were blotted for Polθ and MCM7 alongside a serial dilution of mock-depleted extracts. Asterisk, background band.

(B) LacR-bound p[*lacO*$_{48}$] was replicated in mock-depleted or Polθ-depleted extracts with or without B1-CDK1 treatment. Total DNA replication and ARP are quantified in Figure S3F.

(C) pDPC was replicated in mock-depleted or Polθ-depleted egg extracts with or without B1-CDK1 treatment. Total DNA replication and ARP are quantified in Figure S3G.

(D) Structure of clones derived from mitotic ARPs in mock- or Polθ-depleted extracts. LacR-bound p[*lacO*$_{48}$] was replicated in mock- or Polθ-depleted extracts with B1-CDK1 treatment. Shown is the smear of ~3- to 4-kb mitotic DNA replication products generated after AlwNI digestion was self-ligated, cloned, and sequenced. Elements in the box at the bottom show the sequences of *lacO* and spacers.

(E) Comparison of mitotic ARP-derived clones in the presence or absence of Polθ. Mock depletion (Figure 2D) and Polθ depletion (Figure S3H) in experiment 1 (Exp. 1) were performed independently, whereas they were performed side by side (Figure 3D) in Exp. 2. The p value was from an unpaired two-tailed Student's t test.
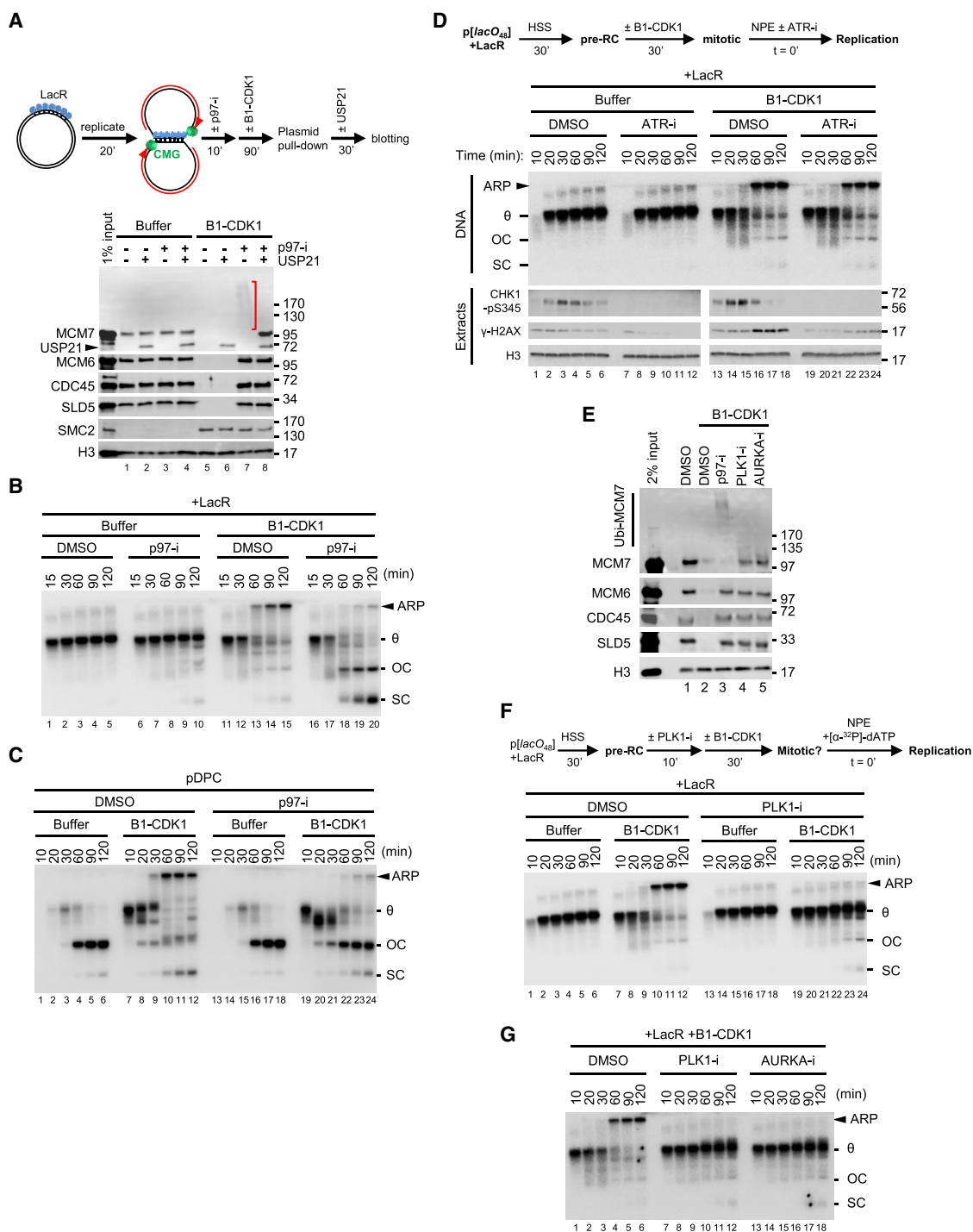
See also Figure S3.

Figure 4. Mitotic CDK-Induced Fork Collapse Requires p97-Dependent CMG Unloading

(A) The LacR-bound p[*lacO*$_{48}$] plasmid was replicated and treated as schemed. Chromatin-bound proteins were recovered and blotted with the indicated antibodies. Red bracket, ubiquitylated MCM7. Histone H3 served as a loading control. Note that the MCM7 antibody cross-reacts with USP21.

(B) LacR-bound p[*lacO*$_{48}$] was replicated in the presence or absence of p97-i and B1-CDK1, as indicated.

(C) pDPC was replicated in the presence or absence of p97-i and B1-CDK1, as indicated. ARP, OC+SC, and overall DNA replication are quantified in Figure S4G.

(D) Effect of ATR inhibition on stalled replication forks. The LacR-bound p[*lacO*$_{48}$] plasmid was replicated as schemed. The final concentration of the ATR inhibitor (ATR-i; ETP-46464) in the reactions was 200 μM. Extracts with [α-^{32}P]-deoxyadenosine triphosphate (dATP) were sampled to track DNA replication, whereas extracts without [α-^{32}P]-dATP were sampled in parallel to track CHK1-S345 phosphorylation (CHK1-pS345), γ-H2AX. Histone H3 was included as a loading control.

(legend continued on next page)

phosphorylation (γ-H2AX) signal, consistent with inhibition of DSB formation (Figure S4F, compare lanes 13–18 and 19–24). As seen for the LacR plasmid, p97-i also prevented ARP formation on pDPC (Figures 4C and S4G). Our data demonstrate that breakage of stalled forks in the presence of mitotic CDK requires p97 activity.

B1-CDK1-Induced Fork Breakage Requires PLK1 and AURKA but Not Inhibition of ATR Signaling

In mammalian cells, inhibition of ATR signaling leads to fork breakage and chromosomal fragmentation that depends on the protein kinases CDK1, PLK1, and AURKA (Aurora kinase A) (Brown and Baltimore, 2000; Ragland et al., 2013). We therefore examined whether these kinases affect fork breakage in egg extracts. As shown in Figure 4D, a potent ATR inhibitor (ATR-i, ETP-46464) did not induce breakage of forks stalled at a LacR array in interphase egg extract lacking B1-CDK1 (measured by ARP formation), even though ATR-i abolished CHK1-pS345 and γ-H2AX (lanes 7–12). Conversely, the fork breakage observed in the presence of B1-CDK1 occurred even though ATR signaling was active, as seen from CHK1-pS345 (Figure 4D, lanes 13–18), and ATR-i did not further enhance breakage in this setting (Figure 4D, lanes 19–24). Therefore, in interphase egg extract, ATR inhibition is insufficient to cause fork breakage, and in mitotic extract, B1-CDK1 induces fork breakage in the presence of ATR activity. Strikingly, B1-CDK1-induced CMG ubiquitylation, CMG unloading, and fork breakage were all suppressed by selective inhibitors of PLK1 or AURKA (Figures 4E–4G). We conclude that, in egg extracts that are arrested in a mitotic state, ATR is unable to suppress fork breakage, whereas breakage depends on PLK1 and AURKA, consistent with findings in mammalian cells (Ragland et al., 2013).

B1-CDK1 Induces p97-Dependent Replication Fork Collapse

Replication fork collapse is defined as a state from which replication cannot restart, and we wanted to determine whether B1-CDK1 induces such a state in egg extracts. As we showed previously (Dewar et al., 2015), replication forks stalled at a LacR array are able to resume synthesis upon addition of IPTG, leading to mature, supercoiled replication products (Figure S4H, lanes 7–12). In the presence of B1-CDK1, IPTG treatment did not generate mature replication products (Figure S4H, lanes 19–24), presumably because forks broke and underwent end joining. However, when p97i was included with B1-CDK1, mature replication products were fully recovered after IPTG addition (Figure S4H, lanes 31–36). Thus, B1-CDK1 induces collapse of stalled replication forks, and inhibition of p97 is sufficient to prevent this collapse.

TRAIP Promotes B1-CDK1-Induced CMG Unloading at Stalled Forks

We next sought the E3 ubiquitin ligase responsible for B1-CDK1-dependent CMG unloading. Although the Cullin inhibitor MLN-4924 (Cul-i) blocked CMG unloading during replication termination in interphase (Figure S5A, compare lanes 1 and 4) (Dewar et al., 2017), it had almost no effect on mitotic CMG unloading from stalled forks (Figure S5A, compare lanes 3 and 6), indicating that the latter process does not involve CRL2^{Lrr1} or any other Cullin-ring ligase.

The E3 ubiquitin ligase TRAIP counteracts replication stress to maintain genome integrity (Feng et al., 2016; Harley et al., 2016; Hoffmann et al., 2016; Soo Lee et al., 2016). TRAIP is bound to replication forks that have stalled at a LacR array (Dewar et al., 2017), and it promotes CMG ubiquitylation and unloading when forks converge on ICLs (Wu et al., 2019). Strikingly, immunodepletion of TRAIP from egg extract (Figure 5A) prevented B1-CDK1-induced CMG unloading at stalled forks (Figure 5B, compare lanes 2 and 6), and it eliminated polyubiquitylation of MCM7 in the presence of p97-i (Figure 5B, compare lanes 4 and 8). Furthermore, TRAIP depletion abolished the formation of ARPs during replication of the LacR plasmid (Figure 5C, compare lanes 7–12 and 19–24) and pDPC (Figure S5B). Re-addition of recombinant wild-type TRAIP (rTRAIP^{WT}) purified from bacteria to TRAIP-depleted egg extracts rescued the formation of mitotic ARPs (Figure 5D; Figures S5C–S5E). We also added back rTRAIP^{R18C}, a point mutant of TRAIP that was identified in a human patient with primordial dwarfism (Harley et al., 2016). Unlike rTRAIP^{WT}, rTRAIP^{R18C} supported only low levels of ARP formation on the LacR plasmid (Figure 5D, compare lanes 19–24 and 13–18). rTRAIP^{ΔPIP} lacking its C-terminal PCNA interaction motif (PCNA interacting peptide [PIP] box, amino acids 460–469) induced mitotic ARPs as efficiently as rTRAIP^{WT} (Figure S5F), consistent with TRAIP's PIP box being dispensable for the suppression of genome instability in mammalian cells (Hoffmann et al., 2016). We conclude that, in the context of stalled forks, TRAIP is essential for mitotic CDK-induced CMG unloading and fork collapse.

Chromatin Recruitment of TRAIP Is Not Regulated by B1-CDK1

To understand how TRAIP is regulated, we monitored its binding to chromatin. As we showed previously (Dewar et al., 2017), in interphase egg extract, TRAIP is associated with replisomes that have stalled at a LacR array (Figure 5B, lane 1). Therefore, TRAIP is present at forks before they are exposed to B1-CDK1. Upon addition of B1-CDK1, TRAIP was lost from the chromatin, but not when CMG unloading was inhibited with p97-i (Figure 5B, compare lanes 2 and 4). Interestingly, chromatin-bound TRAIP

(E) The LacR-bound p[*lacO₄₈*] plasmid was replicated and treated as in (A). The final concentrations of PLK1 inhibitor (PLK1-i, BI-2536) and Aurora kinase A inhibitor (AURKA-i, MLN-8237) were 50 μM and 10 μM, respectively. DMSO and p97-i treatments were included as controls. Chromatin-bound proteins were recovered and blotted with the indicated antibodies.

(F) LacR-bound p[*lacO₄₈*] was replicated as schemed. PLK1-i was added 10 min before B1-CDK1 treatment, with a final concentration of 50 μM in the overall reaction.

(G) LacR-bound p[*lacO₄₈*] was replicated in the presence of PLK1-i or AURKA-i, as schemed in (F). The final concentrations of PLK1-i and AURKA-i were 50 μM and 10 μM, respectively.
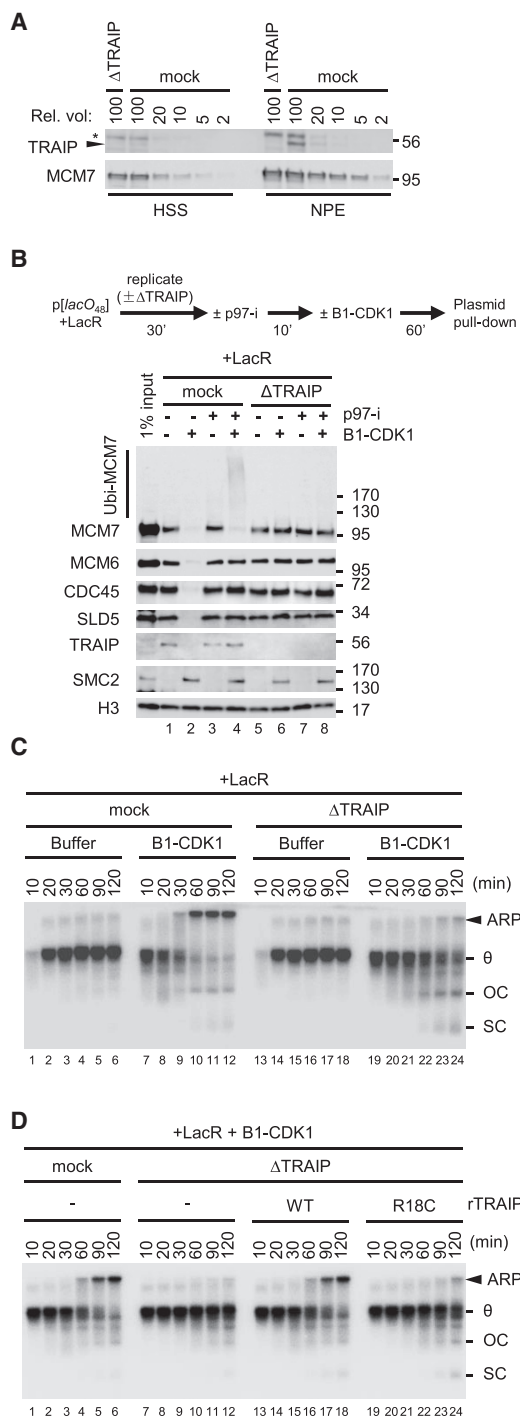
See also Figure S4.

did not increase in the presence of B1-CDK1 and p97-i compared with the level observed before B1-CDK1 addition (Figure 5B, compare lanes 1 and 4). These data suggest that mitotic CDK activates TRAIP in a manner that does not involve its *de novo* recruitment to the fork.

Fork Breakage in Mitotic Extracts Is Distinct from Programmed Incisions during ICL Repair

As seen for B1-CDK1-induced fork breakage (Figure 5), incision of forks that have converged on cisplatin ICLs in interphase egg extracts requires TRAIP (Wu et al., 2019). We therefore asked whether mitotic fork breakage also requires FANCI-FANCD2, XPF-ERCC1, or SLX1-SLX4, which promote DNA incisions during ICL repair (Klein Douwel et al., 2014; Knipscheer et al., 2009). Immunodepletion of FANCI-FANCD2 did not prevent mitotic ARP formation on the LacR plasmid (Figures S5G and S5H), nor did depletion of SLX4, XPF, or MUS81 (data not shown). We speculate that there might be redundancy among SLX1, XPF, and MUS81 for mitotic fork breakage or that other nucleases are involved. Our results indicate that, although ICL incisions and B1-CDK1-dependent replication fork collapse both appear to require TRAIP-dependent CMG unloading, these processes are otherwise mechanistically distinct.

TRAIP Promotes CMG Unloading from Terminated Replisomes in Mitosis

In *C. elegans* early embryos lacking CUL2[LRR-1], CMGs persist on chromatin until late prophase, when they are unloaded from chromatin by p97 (Sonneville et al., 2017). This observation indicated that an alternative ubiquitylation pathway acts to unload terminated CMGs in mitosis, but the relevant E3 ubiquitin ligase has not been identified. To determine whether TRAIP is involved in this pathway, we first addressed whether *Xenopus* egg extracts recapitulate mitotic unloading of CMGs that have undergone replication termination. To this end, we replicated a plasmid in interphase egg extracts in the presence of Cul-i. DNA synthesis went to completion (Figure S6A), but CMG unloading was blocked because of inhibition of CRL2[Lrr1] (Figure 6A, compare lanes 1 and 2; Dewar et al., 2017). Importantly, upon addition of B1-CDK1, CMG was unloaded despite the presence of Cul-i (Figure 6A, lane 6), and this unloading was blocked by p97-i (Figure 6A, lane 8). Therefore, as seen in worms, mitotic frog egg extracts support CRL2[Lrr1]-independent unloading of terminated CMGs. Interestingly, in the presence of p97-i, MCM7 was ubiquitylated even more extensively than in interphase extracts (Figure 6A, compare lanes 7 and 8 and 3 and 4; Figure S6B, compare lanes 5 and 6 and 1 and 2). This hyper-ubiquitylation was

Figure 5. The E3 Ubiquitin Ligase TRAIP Promotes Mitotic CMG Unloading from a Stalled Replication Fork

(A) Mock-depleted and TRAIP-depleted egg extracts were blotted for TRAIP and MCM7 alongside a serial dilution of mock-depleted extracts. Asterisk, background band.

(B) The LacR-bound p[*lacO48*] plasmid was replicated in mock-depleted or TRAIP-depleted egg extracts and treated as schemed. Chromatin-bound proteins were recovered and blotted with the indicated antibodies.

(C) LacR-bound p[*lacO48*] was replicated in mock-depleted or TRAIP-depleted extracts with or without B1-CDK1 treatment.

(D) LacR-bound p[*lacO48*] was replicated in mitotic mock-depleted or TRAIP-depleted egg extracts with or without recombinant wild-type TRAIP (rTRAIP[WT]) or R18C mutant (rTRAIP[R18C]), as indicated. rTRAIP[WT] and rTRAIP[R18C] were added to NPE at a concentration of 21 ng/μL (~7-fold over endogenous TRAIP; see quantification in Figure S5C). Matched buffer without recombinant protein was added to control reactions. Addition of rTRAIP[WT] at the endogenous level (Figure S5C) into TRAIP-depleted extracts also led to substantial rescue of mitotic ARPs (Figures S5D and S5E).
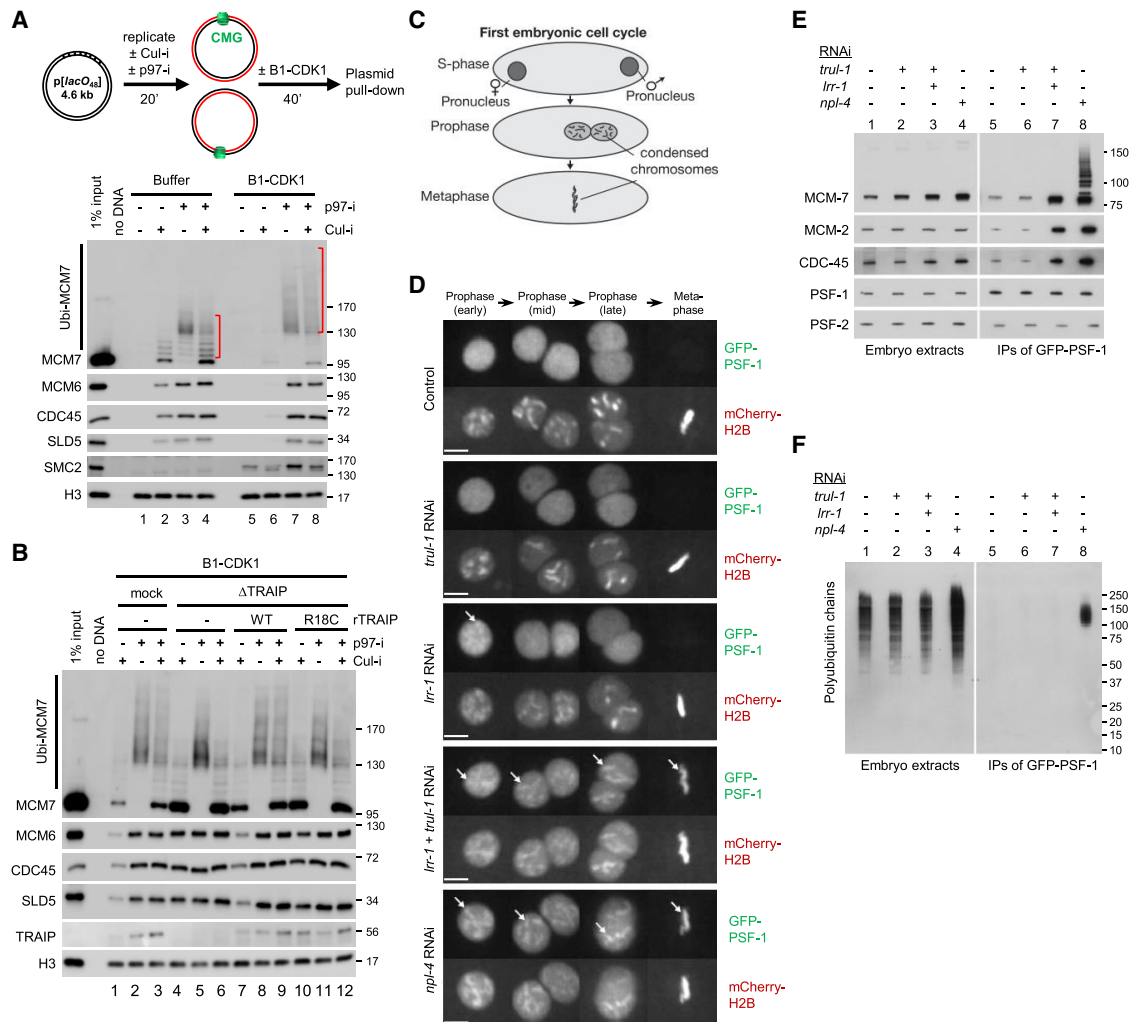
See also Figure S5.

Figure 6. TRAIP Mediates Unloading of Terminated CMGs in Mitosis

(A) The p[$lacO_{48}$] plasmid, in the absence of LacR, was replicated and treated as schemed. Chromatin-bound proteins were recovered and blotted with the indicated antibodies. Red brackets indicate the levels of MCM7 ubiquitylation.

(B) The p[$lacO_{48}$] plasmid, in the absence of LacR, was replicated in mock-depleted or TRAIP-depleted egg extracts supplemented with or without rTRAIP^{WT} (~4-fold of endogenous TRAIP) or rTRAIP^{R18C} (~9-fold of endogenous TRAIP), followed by the indicated treatments. Chromatin-bound proteins were recovered and blotted with the indicated antibodies.

(C) Illustration of the first cell cycle of the *C. elegans* embryo. Following S phase, the female and male pronuclei migrate toward each other, and chromosomes condense during prophase. Subsequently, the two sets of chromosomes intermingle during metaphase.

(D) Time-lapse video microscopy of the first embryonic mitosis in embryos exposed to the indicated RNAi and expressing GFP-PSF-1 and mCherry-histone H2B. The female pronucleus is shown during early prophase, before convergence with the male pronucleus (mid-prophase and late prophase). The arrows indicate examples of persistence of GFP-PSF-1 on condensed chromatin during mitosis. Scale bar, 5 μm.

(E and F) Worms in which the PSF-1 subunit of the CMG helicase was tagged with GFP were subjected to the indicated RNAi treatment. GFP-PSF-1 was recovered by immunoprecipitation, and the association of the indicated proteins was then monitored by immunoblotting against the indicated proteins (E) or ubiquitin (F).

See also Figure S6.

unaffected by Cul-i (Figure 6A, lane 8), indicating that it is CRL2^{Lrr1}-independent. Importantly, TRAIP depletion inhibited B1-CDK1-induced CMG unloading from terminated forks (Figure 6B, compare lanes 1 and 4; Figure S6C, compare lanes 1 and 4) and MCM7 hyper-ubiquitylation in the presence of p97-i (Figure 6B, compare lanes 2 and 5 as well as lanes 3 and 6). These defects were reversed by rTRAIP^{WT} but not rTRAIP^{R18C}

(Figures 6B and S6C). Therefore, in the absence of CRL2^{Lrr1} activity, TRAIP promotes an alternative pathway to unload terminated CMGs in mitotic egg extract.

We next asked whether the *C. elegans* ortholog of TRAIP, which we called TRUL-1 (Traip Ubiquitin Ligase 1, encoded by the previously uncharacterized *C. elegans* gene B0432.13), controls mitotic removal of CMG from chromatin in the first
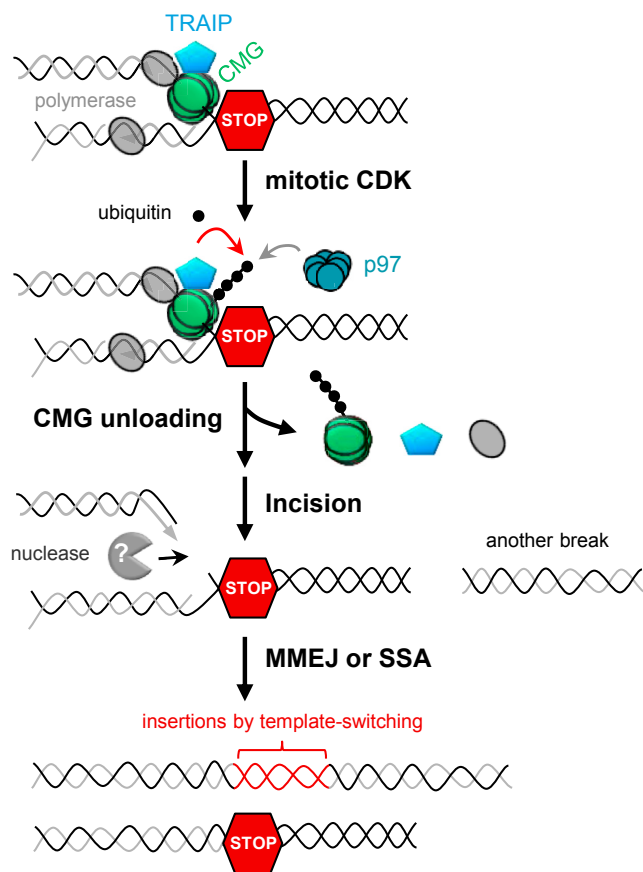
Figure 7. Model of CMG Unloading, Fork Breakage, and Complex DNA Rearrangements upon Premature Mitotic Entry

When a replication fork encounters a replication barrier (indicated as a red hexagonal stop sign), the replisome containing CMG and TRAIP is stably stalled during interphase. With the increase of mitotic CDK activity, the E3 ubiquitin ligase TRAIP is activated (directly or indirectly) to cause CMG ubiquitylation on the MCM7 subunit, which, in turn, triggers CMG unloading from chromatin by CDC48 or p97 ATPase. Loss of CMG leads to incision by so far unknown DNA nuclease(s), followed by error-prone double-strand repair by MMEJ and/or single-strand annealing (SSA), which results in DNA rearrangements such as deletions and insertions from template-switching events. See also Figure S7.

embryonic cell cycle (Figure 6C). On its own, RNAi depletion of TRUL-1 had no effect on CMG disassembly. However, simultaneous depletion of TRUL-1 and LRR-1 led to the persistence on mitotic chromatin of the PSF-1 subunit of GINS (Figure 6D, four of five embryos examined) and CDC-45 (Figure S6D, five of five embryos examined), indicating that *C. elegans* TRAIP is required for the removal of CMG from mitotic chromatin in animals. Moreover, compared with single depletion of TRUL-1 or LRR-1, double depletion led to the accumulation of CMG complexes containing unmodified MCM7 (Figure 6E, lane 7). This contrasts with the persistence of ubiquitylated CMGs observed upon depletion of p97's cofactor NPL-4 (Figures 6E and 6F, lane 8) (Sonneville et al., 2017). Thus, unloading of terminated CMGs in mitosis is a conserved function of TRAIP in metazoans.

DISCUSSION

The molecular events underlying mitotic replication fork breakage and how such breakage affects genome stability remain unclear. Here we show that, in mitotic egg extracts, the E3 ubiquitin ligase TRAIP promotes p97-dependent replisome disassembly, followed by replication fork breakage and end joining events involving SSA and MMEJ (Figure 7). As discussed below, we propose that TRAIP-dependent fork breakage can be beneficial or detrimental, depending primarily on the burden of stressed forks at mitotic entry.

TRAIP's regulation of CMG ubiquitylation is critically dependent on cell cycle status. In the presence of B1-CDK1, TRAIP targets stalled CMGs, which encircle single-stranded DNA (ssDNA), and terminated CMGs, which probably encircle double-stranded DNA (dsDNA) (Figures S6Ei and S6Eii; Dewar et al., 2015). In contrast, TRAIP's action in interphase extracts is more selective. In this setting, TRAIP does not target terminated CMGs, a function performed by CRL2^Lrr1 in S phase (Figure S6Eiii; Dewar et al., 2017; Sonneville et al., 2017), nor does TRAIP appear to target CMG at single moving or stalled forks, which would cause premature fork collapse. However, TRAIP does target CMGs that have converged at an ICL in interphase (Wu et al., 2019), leading us to speculate that in mitosis, B1-CDK1-induces a conformational change in TRAIP that allows it to ubiquitylate any CMG that remains on chromatin.

It has been widely proposed that replisome disassembly causes fork collapse (Cortez, 2015; Toledo et al., 2017), but without knowing the mechanism of disassembly, testing this idea has been difficult. Here we show that B1-CDK1 induces CMG ubiquitylation and unloading, fork breakage, and fork collapse. This cascade is inhibited via multiple independent manipulations (PLK1-i, p97-i, and TRAIP depletion) that all target the CMG unloading step. Thus, our data establish a firm relationship between replisome disassembly, fork breakage, and collapse in a vertebrate cell-free system that exhibits physiological complexity. Whether the inability to restart the fork (collapse) results from replisome disassembly per se or a downstream event such as fork breakage is presently unclear. Moreover, without active recombinant MCM2-7, we cannot make point mutations to directly test whether CMG ubiquitylation is responsible for fork breakage. Nevertheless, multiple lines of evidence point to CMG as the most likely target. First, TRAIP associates with stalled and terminated replication forks (Dewar et al., 2017; Hoffmann et al., 2016), ideally positioning TRAIP for CMG ubiquitylation. Second, prior to fork collapse, B1-CDK1 induces rapid and quantitative ubiquitylation of MCM7, the same protein that is ubiquitylated when CMG is unloaded during replication termination. Finally, CMG is unique among replisome components in that it cannot be reloaded *de novo* in S phase (Deegan and Diffley, 2016). Thus, loss of CMG provides a simple explanation for the irreversibility of fork collapse. It will be interesting to determine how this pathway relates to the depletion of RPA at the fork, which has also been proposed to trigger fork collapse and breakage (Toledo et al., 2013).

After fork breakage in mitotic extracts, the newly formed DNA ends undergo two classes of joining events. The first class involves deletions of the highly repetitive *lacO* repeats and is

thus best explained by SSA. SSA, which is usually RAD52 dependent (Bhargava et al., 2016), has recently been shown to mediate DNA repair synthesis during mitosis (Bhowmick et al., 2016). However, we have not been able to test the involvement of RAD52 because of an inability to raise antibodies against *Xenopus* RAD52. The second class of end joining products is mediated by micro-homology, sometimes with multiple template-switching events, indicative of MMEJ (Wyatt et al., 2016). Consistent with this idea, ARPs were reduced and complex rearrangements were eliminated in Polθ-depleted extracts. Notably, we detected only short-tract template switches typical of MMEJ. If template-switching events mediated by Polθ or other factors were followed by more processive DNA synthesis near the break, then duplications could result that resemble copy number alterations in human cancer and congenital disease (Carvalho and Lupski, 2016; Leibowitz et al., 2015).

We envision at least two beneficial effects of TRAIP-dependent replisome disassembly in mitosis. One arises when converging forks are unable to complete DNA replication by anaphase, as seen at CFSs (West and Chan, 2017). We propose that TRAIP-dependent CMG unloading leads to preferential breakage on the two leading strand templates because these are normally protected by CMG (Fu et al., 2011) and, therefore, exposed after CMG dissociation (Figure S7). In this scenario, one intact daughter chromosome would immediately be restored by gap filling, and the other could be regenerated via joining of the two broken ends, albeit with sister chromatid exchange and at the cost of a small deletion (Figure S7, left branch). Importantly, this mechanism avoids the formation of acentric and dicentric chromosomes that would result if the forks underwent random breakage (Figure S7, right branch), thus biasing breakage at CFSs toward more beneficial outcomes. Strikingly, CFS expression induces chromosomal alterations that exhibit key features predicted by our model: submicroscopic deletions covering the CFS locus, microhomologies at the breakpoint junctions, and a very high frequency of sister chromatid exchanges (Glover et al., 2017; Figure S7, left branch). In contrast, break-induced replication models of CFS expression (Bhowmick et al., 2016; Minocherhomji et al., 2015) do not account for the sister chromatid exchanges at CFSs, and they would not be beneficial at CFSs located distant from chromosome ends. A second possible benefit of TRAIP activity in mitosis is to disassemble terminated CMGs that evaded the action of CRL2^{Lrr1} in the previous S phase. In principle, such CMGs might interfere with transcription, replication, or other processes in the next cell cycle. Future studies will address whether the dwarfism phenotype observed in patients with TRAIP mutations (Harley et al., 2016) is caused by defective CMG unloading in mitosis or other TRAIP-dependent processes.

In addition to its beneficial effects, we propose that TRAIP-dependent CMG unloading contributes to genome instability phenomena that were previously linked to mitotic DNA replication. These include chromosome breakage after S and M phase cells are fused (Duelli et al., 2007; Johnson and Rao, 1970; Rao et al., 1982) or when mitotic CDK is prematurely activated in S phase by WEE1 inhibition (Domínguez-Kelly et al., 2011; Duda et al., 2016), and chromothripsis in micronuclei that are still engaged in replication when they enter mitosis (Crasta et al., 2012; Leibowitz et al., 2015; Ly et al., 2017). In these cases,

massive chromosomal breakage leads to genome instability or cell death. Notably, chromosome fragmentation in the presence of the WEE1 inhibitor and common fragile site expression are both MUS81-dependent (Domínguez-Kelly et al., 2011; Duda et al., 2016; Naim et al., 2013; Ying et al., 2013). In contrast, fork breakage in our experiments was not inhibited by MUS81 depletion. Whether this reflects incomplete MUS81 depletion in extracts, greater redundancy with other nucleases, or a difference in experimental systems remains to be determined.

Many studies of fork collapse focus on its regulation by ATR. Although ATR-dependent phosphorylation of SMARCAL1 and WRN regulates fork stability, these ATR substrates do not appear to account for ATR's essential role in preventing fork collapse (Cortez, 2015; Pasero and Vindigni, 2017; Saldivar et al., 2017). Instead, a growing body of evidence suggests that ATR affects fork stability indirectly (Toledo et al., 2017). For example, ATR inhibition of late origin firing prevents exhaustion of the nuclear RPA pool, causing fork deprotection and breakage (Toledo et al., 2013). However, given the concentration of RPA in egg extracts (∼10 μM; Walter et al., 1998; Wühr et al., 2015) and the concentration of DNA in our experiments, RPA exhaustion cannot account for our results. Another hypothesis to explain the effect of ATR on fork stability involves the suppression of mitotic kinases. In cells treated with APH and ATR-i, replication fork collapse depends on B1-CDK1, AURKA, and PLK1 (Eykelenboom et al., 2013; Ragland et al., 2013). Even in the absence of exogenous replication stress, ATR prevents premature accumulation of Cyclin B and PLK1 in S phase, which is critical to suppress replication fork collapse and genome instability (Ruiz et al., 2016; Saldivar et al., 2018). Thus, replication fork collapse in interphase can be due to premature activation of mitotic kinases. Consistent with the central importance of ATR in restraining B-CDK1, ATR is not required to stabilize stalled DNA replication forks in egg extracts that are permanently arrested in interphase (Figure 4D; Luciani et al., 2004). Conversely, when stressed forks are exposed to B1-CDK1, forks break, even in the presence of ATR activity. Based on these considerations, in many studies where ATR inhibition induces replication fork collapse, this collapse may be due to premature activation of B1-CDK1 and TRAIP-dependent replisome disassembly.

In summary, our data suggest that, when TRAIP is activated by mitotic CDK, a short temporal window opens in which replication forks can finish replication and terminate. The window closes when CMGs are ubiquitylated and extracted from chromatin. In the presence of a few unreplicated loci (e.g., fragile sites), CMG unloading and fork breakage promote chromosome segregation and genome integrity, but when many forks are present (e.g., micronuclei, premature CDK1 activation in S phase), massive DNA fragmentation results, leading to cell death or transformation.

STAR★METHODS

Detailed methods are provided in the online version of this paper and include the following:

- KEY RESOURCES TABLE
- CONTACT FOR REAGENT AND RESOURCE SHARING

- ● EXPERIMENTAL MODEL AND SUBJECT DETAILS
  - ○ Xenopus laevis
  - ○ *C. elegans* maintenance
- ● METHOD DETAILS
  - ○ Protein purification
  - ○ DNA constructs
  - ○ *Xenopus* egg extracts and DNA replication
  - ○ Immunodepletion and western blotting
  - ○ Sperm chromatin spin-down assay
  - ○ Plasmid pull-down assay
  - ○ De-ubiquitination assay
  - ○ Restriction digestion
  - ○ Sequencing
  - ○ RNA interference
  - ○ Microscopy
  - ○ Extracts of worm embryos and immunoprecipitation of protein complexes
  - ○ Data quantification

AUTHOR CONTRIBUTIONS

D.P. initiated the project. L.D., D.P., and J.C.W. designed the experiments, interpreted the results, and prepared the manuscript. R.A.W. contributed recombinant TRAIP proteins and obtained initial evidence that TRAIP is required for ARP formation. R.S. performed and K.L. directed experiments in worms (Figures 6C–6F and S6D). O.V.K. contributed Figures 6A, 6B, and S6A–S6C. L.D. performed all other experiments.

DECLARATION OF INTERESTS

The authors declare no competing interests.

REFERENCES

Amunugama, R., Willcox, S., Wu, R.A., Abdullah, U.B., El-Sagheer, A.H., Brown, T., McHugh, P.J., Griffith, J.D., and Walter, J.C. (2018). Replication Fork Reversal during DNA Interstrand Crosslink Repair Requires CMG Unloading. Cell Rep. *23*, 3419–3428.

Baumann, C., Körner, R., Hofmann, K., and Nigg, E.A. (2007). PICH, a centromere-associated SNF2 family ATPase, is regulated by Plk1 and required for the spindle checkpoint. Cell *128*, 101–114.

Bhargava, R., Onyango, D.O., and Stark, J.M. (2016). Regulation of Single-Strand Annealing and its Role in Genome Maintenance. Trends Genet. *32*, 566–575.

Bhowmick, R., and Hickson, I.D. (2017). The "enemies within": regions of the genome that are inherently difficult to replicate. F1000Res. *6*, 666.

Bhowmick, R., Minocherhomji, S., and Hickson, I.D. (2016). RAD52 Facilitates Mitotic DNA Synthesis Following Replication Stress. Mol. Cell *64*, 1117–1126.

Blow, J.J., and Laskey, R.A. (1986). Initiation of DNA replication in nuclei and purified DNA by a cell-free extract of Xenopus eggs. Cell *47*, 577–587.

Brenner, S. (1974). The genetics of Caenorhabditis elegans. Genetics *77*, 71–94.

Brown, E.J., and Baltimore, D. (2000). ATR disruption leads to chromosomal fragmentation and early embryonic lethality. Genes Dev. *14*, 397–402.

Budzowska, M., Graham, T.G., Sobeck, A., Waga, S., and Walter, J.C. (2015). Regulation of the Rev1-pol ζ complex during bypass of a DNA interstrand cross-link. EMBO J. *34*, 1971–1985.

Carvalho, C.M., and Lupski, J.R. (2016). Mechanisms underlying structural variant formation in genomic disorders. Nat. Rev. Genet. *17*, 224–238.

Chan, K.L., North, P.S., and Hickson, I.D. (2007). BLM is required for faithful chromosome segregation and its localization defines a class of ultrafine anaphase bridges. EMBO J. *26*, 3397–3409.

Cortez, D. (2015). Preventing replication fork collapse to maintain genome integrity. DNA Repair (Amst.) *32*, 149–157.

Crasta, K., Ganem, N.J., Dagher, R., Lantermann, A.B., Ivanova, E.V., Pan, Y., Nezi, L., Protopopov, A., Chowdhury, D., and Pellman, D. (2012). DNA breaks and chromosome pulverization from errors in mitosis. Nature *482*, 53–58.

De Piccoli, G., Katou, Y., Itoh, T., Nakato, R., Shirahige, K., and Labib, K. (2012). Replisome stability at defective DNA replication forks is independent of S phase checkpoint kinases. Mol. Cell *45*, 696–704.

Deegan, T.D., and Diffley, J.F. (2016). MCM: one ring to rule them all. Curr. Opin. Struct. Biol. *37*, 145–151.

Dewar, J.M., Budzowska, M., and Walter, J.C. (2015). The mechanism of DNA replication termination in vertebrates. Nature *525*, 345–350.

Dewar, J.M., Low, E., Mann, M., Räschle, M., and Walter, J.C. (2017). CRL2^Lrr1 promotes unloading of the vertebrate replisome from chromatin during replication termination. Genes Dev. *31*, 275–290.

Domínguez-Kelly, R., Martín, Y., Koundrioukoff, S., Tanenbaum, M.E., Smits, V.A., Medema, R.H., Debatisse, M., and Freire, R. (2011). Wee1 controls genomic stability during replication by regulating the Mus81-Eme1 endonuclease. J. Cell Biol. *194*, 567–579.

Duda, H., Arter, M., Gloggnitzer, J., Teloni, F., Wild, P., Blanco, M.G., Altmeyer, M., and Matos, J. (2016). A Mechanism for Controlled Breakage of Under-replicated Chromosomes during Mitosis. Dev. Cell *39*, 740–755.

Duelli, D.M., Padilla-Nash, H.M., Berman, D., Murphy, K.M., Ried, T., and Lazebnik, Y. (2007). A virus causes cancer by inducing massive chromosomal instability through cell fusion. Curr. Biol. *17*, 431–437.

Dungrawala, H., Rose, K.L., Bhat, K.P., Mohni, K.N., Glick, G.G., Couch, F.B., and Cortez, D. (2015). The Replication Checkpoint Prevents Two Types of Fork Collapse without Regulating Replisome Stability. Mol. Cell *59*, 998–1010.

Duxin, J.P., Dewar, J.M., Yardimci, H., and Walter, J.C. (2014). Repair of a DNA-protein crosslink by replication-coupled proteolysis. Cell *159*, 346–357.

El Achkar, E., Gerbault-Seureau, M., Muleris, M., Dutrillaux, B., and Debatisse, M. (2005). Premature condensation induces breaks at the interface of early and late replicating chromosome bands bearing common fragile sites. Proc. Natl. Acad. Sci. USA *102*, 18069–18074.

Eykelenboom, J.K., Harte, E.C., Canavan, L., Pastor-Peidro, A., Calvo-Asensio, I., Llorens-Agost, M., and Lowndes, N.F. (2013). ATR activates the S-M checkpoint during unperturbed growth to ensure sufficient replication prior to mitotic onset. Cell Rep. *5*, 1095–1107.

Feng, W., Guo, Y., Huang, J., Deng, Y., Zang, J., and Huen, M.S. (2016). TRAIP regulates replication fork recovery and progression via PCNA. Cell Discov. 2, 16016.

Fu, Y.V., Yardimci, H., Long, D.T., Ho, T.V., Guainazzi, A., Bermudez, V.P., Hurwitz, J., van Oijen, A., Schärer, O.D., and Walter, J.C. (2011). Selective bypass of a lagging strand roadblock by the eukaryotic replicative DNA helicase. Cell 146, 931–941.

Fullbright, G., Rycenga, H.B., Gruber, J.D., and Long, D.T. (2016). p97 Promotes a Conserved Mechanism of Helicase Unloading during DNA Cross-Link Repair. Mol. Cell. Biol. 36, 2983–2994.

Glover, T.W., Wilson, T.E., and Arlt, M.F. (2017). Fragile sites in cancer: more than meets the eye. Nat. Rev. Cancer 17, 489–501.

Graham, T.G., Walter, J.C., and Loparo, J.J. (2016). Two-Stage Synapsis of DNA Ends during Non-homologous End Joining. Mol. Cell 61, 850–858.

Harley, M.E., Murina, O., Leitch, A., Higgs, M.R., Bicknell, L.S., Yigit, G., Blackford, A.N., Zlatanou, A., Mackenzie, K.J., Reddy, K., et al. (2016). TRAIP promotes DNA damage response during genome replication and is mutated in primordial dwarfism. Nat. Genet. 48, 36–43.

Hendrickson, M., Madine, M., Dalton, S., and Gautier, J. (1996). Phosphorylation of MCM4 by cdc2 protein kinase inhibits the activity of the minichromosome maintenance complex. Proc. Natl. Acad. Sci. USA 93, 12223–12228.

Hills, S.A., and Diffley, J.F. (2014). DNA replication and oncogene-induced replicative stress. Curr. Biol. 24, R435–R444.

Hoffmann, S., Smedegaard, S., Nakamura, K., Mortuza, G.B., Räschle, M., Ibañez de Opakua, A., Oka, Y., Feng, Y., Blanco, F.J., Mann, M., et al. (2016). TRAIP is a PCNA-binding ubiquitin ligase that protects genome stability after replication stress. J. Cell Biol. 212, 63–75.

Holland, A.J., and Cleveland, D.W. (2012). Chromoanagenesis and cancer: mechanisms and consequences of localized, complex chromosomal rearrangements. Nat. Med. 18, 1630–1638.

Hustedt, N., and Durocher, D. (2016). The control of DNA repair by the cell cycle. Nat. Cell Biol. 19, 1–9.

Johnson, R.T., and Rao, P.N. (1970). Mammalian cell fusion: induction of premature chromosome condensation in interphase nuclei. Nature 226, 717–722.

Kato, H., and Sandberg, A.A. (1968). Chromosome pulverization in human cells with micronuclei. J. Natl. Cancer Inst. 40, 165–179.

Klein Douwel, D., Boonen, R.A., Long, D.T., Szypowska, A.A., Räschle, M., Walter, J.C., and Knipscheer, P. (2014). XPF-ERCC1 acts in Unhooking DNA interstrand crosslinks in cooperation with FANCD2 and FANCP/SLX4. Mol. Cell 54, 460–471.

Knipscheer, P., Räschle, M., Smogorzewska, A., Enoiu, M., Ho, T.V., Schärer, O.D., Elledge, S.J., and Walter, J.C. (2009). The Fanconi anemia pathway promotes replication-dependent DNA interstrand cross-link repair. Science 326, 1698–1701.

Lebofsky, R., Takahashi, T., and Walter, J.C. (2009). DNA replication in nucleus-free Xenopus egg extracts. Methods Mol. Biol. 521, 229–252.

Leibowitz, M.L., Zhang, C.Z., and Pellman, D. (2015). Chromothripsis: A New Mechanism for Rapid Karyotype Evolution. Annu. Rev. Genet. 49, 183–211.

Liu, P., Erez, A., Nagamani, S.C., Dhar, S.U., Kołodziejska, K.E., Dharmadhikari, A.V., Cooper, M.L., Wiszniewska, J., Zhang, F., Withers, M.A., et al. (2011). Chromosome catastrophes involve replication mechanisms generating complex genomic rearrangements. Cell 146, 889–903.

Long, D.T., Räschle, M., Joukov, V., and Walter, J.C. (2011). Mechanism of RAD51-dependent DNA interstrand cross-link repair. Science 333, 84–87.

Luciani, M.G., Oehlmann, M., and Blow, J.J. (2004). Characterization of a novel ATR-dependent, Chk1-independent, intra-S-phase checkpoint that suppresses initiation of replication in Xenopus. J. Cell Sci. 117, 6019–6030.

Lukas, C., Savic, V., Bekker-Jensen, S., Doil, C., Neumann, B., Pedersen, R.S., Grøfte, M., Chan, K.L., Hickson, I.D., Bartek, J., and Lukas, J. (2011). 53BP1 nuclear bodies form around DNA lesions generated by mitotic transmission of chromosomes under replication stress. Nat. Cell Biol. 13, 243–253.

Ly, P., Teitz, L.S., Kim, D.H., Shoshani, O., Skaletsky, H., Fachinetti, D., Page, D.C., and Cleveland, D.W. (2017). Selective Y centromere inactivation triggers chromosome shattering in micronuclei and repair by non-homologous end joining. Nat. Cell Biol. 19, 68–75.

Mankouri, H.W., Huttner, D., and Hickson, I.D. (2013). How unfinished business from S-phase affects mitosis and beyond. EMBO J. 32, 2661–2671.

Minocherhomji, S., Ying, S., Bjerregaard, V.A., Bursomanno, S., Aleliunaite, A., Wu, W., Mankouri, H.W., Shen, H., Liu, Y., and Hickson, I.D. (2015). Replication stress activates DNA repair synthesis in mitosis. Nature 528, 286–290.

Naim, V., Wilhelm, T., Debatisse, M., and Rosselli, F. (2013). ERCC1 and MUS81-EME1 promote sister chromatid separation by processing late replication intermediates at common fragile sites during mitosis. Nat. Cell Biol. 15, 1008–1015.

Pasero, P., and Vindigni, A. (2017). Nucleases Acting at Stalled Forks: How to Reboot the Replication Program with a Few Shortcuts. Annu. Rev. Genet. 51, 477–499.

Peterson, S.E., Li, Y., Chait, B.T., Gottesman, M.E., Baer, R., and Gautier, J. (2011). Cdk1 uncouples CtIP-dependent resection and Rad51 filament formation during M-phase double-strand break repair. J. Cell Biol. 194, 705–720.

Prokhorova, T.A., Mowrer, K., Gilbert, C.H., and Walter, J.C. (2003). DNA replication of mitotic chromatin in Xenopus egg extracts. Proc. Natl. Acad. Sci. USA 100, 13241–13246.

Ragland, R.L., Patel, S., Rivard, R.S., Smith, K., Peters, A.A., Bielinsky, A.K., and Brown, E.J. (2013). RNF4 and PLK1 are required for replication fork collapse in ATR-deficient cells. Genes Dev. 27, 2259–2273.

Rao, P.N., Johnson, R.T., and Sperling, K. (1982). Premature Chromosome Condensation: Application in Basic, Clinical, and Mutation Research (Academic Press).

Räschle, M., Knipscheer, P., Enoiu, M., Angelov, T., Sun, J., Griffith, J.D., Ellenberger, T.E., Schärer, O.D., and Walter, J.C. (2008). Mechanism of replication-coupled DNA interstrand crosslink repair. Cell 134, 969–980.

Räschle, M., Smeenk, G., Hansen, R.K., Temu, T., Oka, Y., Hein, M.Y., Nagaraj, N., Long, D.T., Walter, J.C., Hofmann, K., et al. (2015). DNA repair. Proteomics reveals dynamic assembly of repair complexes during bypass of DNA cross-links. Science 348, 1253671.

Ruiz, S., Mayor-Ruiz, C., Lafarga, V., Murga, M., Vega-Sendino, M., Ortega, S., and Fernandez-Capetillo, O. (2016). A Genome-wide CRISPR Screen Identifies CDC25A as a Determinant of Sensitivity to ATR Inhibitors. Mol. Cell 62, 307–313.

Saldivar, J.C., Cortez, D., and Cimprich, K.A. (2017). The essential kinase ATR: ensuring faithful duplication of a challenging genome. Nat. Rev. Mol. Cell Biol. 18, 622–636.

Saldivar, J.C., Hamperl, S., Bocek, M.J., Chung, M., Bass, T.E., Cisneros-Soberanis, F., Samejima, K., Xie, L., Paulson, J.R., Earnshaw, W.C., et al. (2018). An intrinsic S/G₂ checkpoint enforced by ATR. Science 361, 806–810.

Semlow, D.R., Zhang, J., Budzowska, M., Drohat, A.C., and Walter, J.C. (2016). Replication-Dependent Unhooking of DNA Interstrand Cross-Links by the NEIL3 Glycosylase. Cell 167, 498–511.e14.

Sonneville, R., Querenet, M., Craig, A., Gartner, A., and Blow, J.J. (2012). The dynamics of replication licensing in live Caenorhabditis elegans embryos. J. Cell Biol. 196, 233–246.

Sonneville, R., Moreno, S.P., Knebel, A., Johnson, C., Hastie, C.J., Gartner, A., Gambus, A., and Labib, K. (2017). CUL-2^{LRR-1} and UBXN-3 drive replisome disassembly during DNA replication termination and mitosis. Nat. Cell Biol. 19, 468–479.

Soo Lee, N., Jin Chung, H., Kim, H.J., Yun Lee, S., Ji, J.H., Seo, Y., Hun Han, S., Choi, M., Yun, M., Lee, S.G., et al. (2016). TRAIP/RNF206 is required for recruitment of RAP80 to sites of DNA damage. Nat. Commun. 7, 10463.

Stephens, P.J., Greenman, C.D., Fu, B., Yang, F., Bignell, G.R., Mudie, L.J., Pleasance, E.D., Lau, K.W., Beare, D., Stebbings, L.A., et al. (2011). Massive

genomic rearrangement acquired in a single catastrophic event during cancer development. Cell *144*, 27–40.

Strausfeld, U.P., Howell, M., Descombes, P., Chevalier, S., Rempel, R.E., Adamczewski, J., Maller, J.L., Hunt, T., and Blow, J.J. (1996). Both cyclin A and cyclin E have S-phase promoting (SPF) activity in Xenopus egg extracts. J. Cell Sci. *109*, 1555–1563.

Técher, H., Koundrioukoff, S., Nicolas, A., and Debatisse, M. (2017). The impact of replication stress on replication dynamics and DNA damage in vertebrate cells. Nat. Rev. Genet. *18*, 535–550.

Timmons, L., and Fire, A. (1998). Specific interference by ingested dsRNA. Nature *395*, 854.

Toledo, L.I., Altmeyer, M., Rask, M.B., Lukas, C., Larsen, D.H., Povlsen, L.K., Bekker-Jensen, S., Mailand, N., Bartek, J., and Lukas, J. (2013). ATR prohibits replication catastrophe by preventing global exhaustion of RPA. Cell *155*, 1088–1103.

Toledo, L., Neelsen, K.J., and Lukas, J. (2017). Replication Catastrophe: When a Checkpoint Fails because of Exhaustion. Mol. Cell *66*, 735–749.

Walter, J., and Newport, J. (2000). Initiation of eukaryotic DNA replication: origin unwinding and sequential chromatin association of Cdc45, RPA, and DNA polymerase alpha. Mol. Cell *5*, 617–627.

Walter, J., Sun, L., and Newport, J. (1998). Regulated chromosomal DNA replication in the absence of a nucleus. Mol. Cell *1*, 519–529.

West, S.C., and Chan, Y.W. (2017). Genome Instability as a Consequence of Defects in the Resolution of Recombination Intermediates. Cold Spring Harb. Symp. Quant. Biol. *82*, 207–212.

Wu, R.A., Semlow, D.R., Kamimae-Lanning, A.N., Kochenova, O.V., Chistol, G., Hodskinson, M.R., Amunugama, R., Sparks, J.L., Wang, M., Deng, L., Mimoso, C.A., Low, E., Patel, K.J., and Walter, J.C. (2019). TRAIP is a master regulator of DNA interstrand cross-link repair. Nature. https://doi.org/10.1038/s41586-019-1002-0.

Wühr, M., Güttler, T., Peshkin, L., McAlister, G.C., Sonnett, M., Ishihara, K., Groen, A.C., Presler, M., Erickson, B.K., Mitchison, T.J., et al. (2015). The Nuclear Proteome of a Vertebrate. Curr. Biol. *25*, 2663–2671.

Wyatt, D.W., Feng, W., Conlin, M.P., Yousefzadeh, M.J., Roberts, S.A., Mieczkowski, P., Wood, R.D., Gupta, G.P., and Ramsden, D.A. (2016). Essential Roles for Polymerase θ-Mediated End Joining in the Repair of Chromosome Breaks. Mol. Cell *63*, 662–673.

Ying, S., Minocherhomji, S., Chan, K.L., Palmai-Pallag, T., Chu, W.K., Wass, T., Mankouri, H.W., Liu, Y., and Hickson, I.D. (2013). MUS81 promotes common fragile site expression. Nat. Cell Biol. *15*, 1001–1007.

STAR★METHODS

KEY RESOURCES TABLE

REAGENT or RESOURCE	SOURCE	IDENTIFIER
Antibodies		
Rabbit α-CDC45 (*Xenopus*)	Walter and Newport, 2000	Rabbit# 534
Rabbit α-MCM6 (*Xenopus*)	Semlow et al., 2016	New England Peptide Project# 2926
Rabbit α-MCM7 (*Xenopus*)	Walter and Newport, 2000	Rabbit# 456
Rabbit α-SLD5α (*Xenopus*)	Dewar et al., 2017	N/A
Rabbit α-TRAIP (*Xenopus*)	Dewar et al., 2017	New England Peptide Project# 3472
Rabbit α-FANCD2 (*Xenopus*)	Knipscheer et al., 2009	Rabbit# 20019
Rabbit α-FANCI (*Xenopus*)	Duxin et al., 2014	N/A
Rabbit α-SMC2 (*Xenopus*)	J. Peters lab	N/A
Rabbit α-SMC2 (*Xenopus*)	This study	New England Peptide Project# 3532
Rabbit α-Polθ (*Xenopus*)	Abgent	project# S16042900
Rabbit α-RAD51 (*Xenopus*)	Long et al., 2011	N/A
Rabbit α-XPF (*Xenopus*)	Klein Douwel et al., 2014	N/A
Rabbit α-MUS81 (*Xenopus*)	Klein Douwel et al., 2014	N/A
Rabbit α-SLX4 (*Xenopus*)	Klein Douwel et al., 2014	N/A
Rabbit α-SLX1 (*Xenopus*)	Klein Douwel et al., 2014	N/A
Sheep α-MCM-7 (*C. elegans*)	Sonneville et al., 2017	N/A
Sheep α-MCM-2 (*C. elegans*)	Sonneville et al., 2017	N/A
Sheep α-CDC-45 (*C. elegans*)	Sonneville et al., 2017	N/A
Sheep α-PSF-1 (*C. elegans*)	Sonneville et al., 2017	N/A
Sheep α-PSF-2 (*C. elegans*)	This study	N/A
Mouse α-poly-ubiquitin chains	Enzo Life Sciences	Cat# BML-PW8810; RRID:AB_10541840
Rabbit α-histone H3 (*human*)	Cell Signaling Technology	Cat# 9715S; RRID:AB_331563
Rabbit α-CHK1-pS345 (*human*)	Cell Signaling Technology	Cat# 2348S; RRID:AB_331212
Rabbit α-γH2AX (*human*)	Cell Signaling Technology	Cat# 2577S; RRID:AB_2118010
Bacterial Strains		
Rosetta 2(DE3)pLysS	Novagen	Cat# 71403
T7 Express cells	New England Biolabs	Cat# C2566I
DH5α cells	lab stock	N/A
XL10-Gold cells	Agilent	Cat# 200315
Chemicals		
[α-^{32}P]-dATP	Perkin Elmer	BLU512H500UC
MLN-4924	Active Biochem	Cat# A-1139
NMS-873	Sigma	Cat# SML1128
RO-3306	EMD Millipore	Cat# 217699
BI-2536	Selleckchem	Cat# S1109
MK-5108	Selleck	Cat# S2770
ETP-46464	Sigma	Cat# SML1321
Aphidicolin	Sigma	Cat# A0781-5MG
PHA-767491	Sigma	Cat# PZ0178
NU-7441	Graham et al., 2016	N/A
IPTG (Isopropyl β-D-thiogalactoside)	Sigma	Cat# I5502-10G
Dynabeads M-280	Invitrogen	Cat# 11205D
GFP-Trap_A beads	Chromotek	Cat# gta-100

Continued

REAGENT or RESOURCE	SOURCE	IDENTIFIER
Recombinant Proteins		
Biotinylated LacR	Dewar et al., 2015	N/A
Recombinant TRAIP^WT	This study	N/A
Recombinant TRAIP^R18C	This study	N/A
Recombinant TRAIP^ΔPIP	This study	N/A
BRC peptide	Long et al., 2011	N/A
BRC*** peptide	Long et al., 2011	N/A
Cyclin B1-CDK1	Life Technologies	Cat# PR4768C
Cyclin B1-CDK1	EMD Millipore	Cat# 14-450M
Cyclin A2	Creative Biomart	Cat# CCNA2-6798H
Cyclin E-CDK2	EMD Millipore	Cat# 14-475
USP21	D. Finley lab, and Dewar et al., 2017	N/A
Proteinase K	Roche	Cat# 3115879001
T4 DNA ligase	New England Biolabs	Cat# M0202L
Experimental Models: Organisms/Strains		
Xenopus laevis	Nasco	Cat# LM0053MX
C elegans, TG1754 (GFP-CDC-45)	Sonneville et al., 2012	N/A
C elegans, KAL1 and KAL3 (GFP-PSF-1)	Sonneville et al., 2017	N/A
Oligonucleotides		
ARP-Forward: AAGGCGATTAAGTTGGGTAA	This paper	N/A
ARP-Reverse: CATGTTCTTTCCTGCGTTATCCCCTGA	This paper	N/A
lrr-1-Forward: ATGCGATTACCATGTGAAGTGG	Sonneville et al., 2017	N/A
lrr-1-Reverse: CCTCGTGTGTGTATTCGATATTATC	Sonneville et al., 2017	N/A
trul-1-Forward: ATGACGTCACAGCCCACGTCATC	This paper	N/A
trul-1-Reverse: CGTATTCCGTAAGATTCGACGTA	This paper	N/A
npl-4-Forward: GTCCAAAAGGGCCCAACTGTC	Sonneville et al., 2017	N/A
npl-4-R: CCAGCAGGAACATCCACCAGC	Sonneville et al., 2017	N/A
Recombinant DNA		
pControl for p[lacO48], 4.6 kb	Räschle et al., 2008	N/A
p[lacO48]	K. Vrtis	N/A
pControl for pDPC, 4.3 kb	Duxin et al., 2014	N/A
pDPC	J. Sparks	N/A
pJD152	Dewar et al., 2015	N/A
pET11a[LacR-Avi]	Dewar et al., 2015	N/A
pBirAcm	Dewar et al., 2015	N/A
pH$_6$-SUMO	Graham et al., 2016	N/A
pH$_6$-SUMO-TRAIP	This study	N/A
pH$_6$-SUMO-TRAIP^R18C	This study	N/A
pH$_6$-SUMO-TRAIP^ΔPIP	This study	N/A
L4440 vector	Timmons and Fire, 1998	N/A
Software and Algorithms		
ImageJ	https://fiji.sc/	N/A
Prism	https://www.graphpad.com/	N/A

CONTACT FOR REAGENT AND RESOURCE SHARING

Further information and requests for resources and reagents should be directed to and will be fulfilled by the Lead Contact, Johannes Walter (Johannes_Walter@hms.harvard.edu).

EXPERIMENTAL MODEL AND SUBJECT DETAILS

Xenopus laevis

Egg extracts were prepared using *Xenopus laevis* (Nasco Cat# LM0053MX). All experiments involving animals were approved by the Harvard Medical School Institutional Animal Care and use Committee (IACUC) and conform to relevant regulatory standards.

C. elegans maintenance

The *C. elegans* strains were maintained according to standard procedures (Brenner, 1974) and were grown on 'Nematode Growth Medium' (NGM: 3 g/L NaCl; 2.5 g/L peptone; 20 g/L agar; 5 mg/L cholesterol; 1 mM $CaCl_2$; 1 mM $MgSO_4$; 2.7 g/L KH_2PO_4; 0.89 g/L K_2HPO_4). The following worm strains were used:

    KAL1: psf-1(lab1[gfp::TEV::S-tag::psf-1 + loxP unc-119(+) loxP])
    KAL3: psf-1(lab1); ltIs37[pie-1p::mCherry::his-58 + unc-119(+)]
    TG1754: unc-119(ed3) III; gtIs65[pie-1p::gfp::cdc-45 + unc-119(+)]; ltIs37

METHOD DETAILS

No statistical methods were used to predetermine sample size. All experiments were performed at least twice independently using separate preparations of *Xenopus* egg extracts. A representative result is shown.

Protein purification

To purify biotinylated LacR, the LacR-Avi expressing plasmid pET11a[LacR-Avi] (Avidity, Denver, CO) and biotin ligase expressing plasmid pBirAcm (Avidity, Denver, CO) were co-transformed into T7 Express cells (New England Biolabs). Cultures were supplemented with 50 mM biotin (Research Organics, Cleveland, OH). Expression of LacR-Avi and the biotin ligase was induced by addition of IPTG (Isopropyl β-D-thiogalactoside, Sigma, St. Louis, MO) to a final concentration of 1 mM. Biotinylated LacR-Avi was then purified as described (Dewar et al., 2015). BRC (a ~35 amino acid peptide derived from BRCA2 that binds RAD51) and BRC*** (BRC peptide with mutations at RAD51 binding sites), a gift of K. Vrtis, were purified as reported (Long et al., 2011).

Recombinant TRAIP was expressed in Rosetta 2 (DE3) pLysS (Novagen). Bacteria transformed with His6-SUMO-*X. laevis* TRAIP wild-type (WT), R18C and PIP box mutant (ΔPIP) were grown in media containing 100 μg/mL ampicillin and 27 μg/mL chloramphenicol at 37°C to OD600 0.6, transferred to 16°C for 30 min, and induced overnight with the addition of 0.1 mM IPTG and 50 μM ZnSO4. The bacteria were collected by centrifugation, resuspended in Lysis Buffer (20 mM HEPES-NaOH pH 7.5, 400 mM sodium acetate, 10% glycerol, 20 mM imidazole, 10 μM ZnSO4, 0.1% NP-40, 1 mM DTT, and 1x Roche cOmplete protease inhibitor cocktail), and sonicated. Ammonium sulfate was added to a final concentration of 300 mM, followed by addition of polyethyleneimine to a final concentration of 0.45%. The lysate was rotated for 15 min at 4°C, centrifuged at 40,000 x g for 45 min, and the soluble fraction recovered and precipitated with saturating ammonium sulfate. The precipitated fraction was collected by centrifugation at 40,000 x g for 45 min, resuspended in Lysis Buffer, and rotated for 30 min with NiNTA resin at room temperature. The resin was washed three times with Wash Buffer (20 mM HEPES-NaOH pH 7.5, 400 mM sodium acetate, 10% glycerol, 20 mM imidazole, 10 μM ZnSO4, 0.01% NP-40, 1 mM DTT) and the protein was eluted with Elution Buffer (20 mM HEPES-NaOH pH 7.5, 400 mM sodium acetate, 10% glycerol, 120 mM imidazole, 10 μM ZnSO4, 0.01% NP-40, 1 mM DTT). The SUMO protease Ulp1 was added to the eluate to a final concentration of 0.03 mg/mL and dialyzed against Dialysis Buffer (20 mM HEPES-NaOH pH 7.5, 400 mM sodium acetate, 120 mM imidazole, 10% glycerol) overnight at 4°C. Aliquots were flash frozen and stored at −80°C.

Other proteins used in this study were Cyclin B1-CDK1 (Life Technologies Cat# PR4768C and EMD Millipore Cat# 14-450M), Cyclin A2 (Creative Biomart, Cat# CCNA2-6798H) and Cyclin E-CDK2 (EMD Millipore Cat# 14-475). USP21 was a gift from D. Finley.

DNA constructs

The 4.6 kb p[$lacO_{48}$] plasmid (a generous gift of K. Vrtis) contains an array of 48 *lacO* sites which can be bound by the *lac* repressor (LacR) to form replication barriers. The pDPC plasmid (4.3 kb), a generous gift of J. Sparks, was constructed based on a previous protocol (Duxin et al., 2014). Control plasmid (pControl) used in Figure 1G has the same DNA sequence as pDPC, but lacks crosslinks.

Xenopus egg extracts and DNA replication

Xenopus egg extracts including Low Speed Supernatant (LSS), High Speed Supernatant (HSS), and Nucleoplasmic egg extract (NPE) were prepared as described (Blow and Laskey, 1986; Lebofsky et al., 2009).

To assess the effects of mitotic cyclins, demembranated sperm chromatin from *Xenopus laevis* males was incubated in LSS (4,000 sperms/μL LSS) for 40 minutes at room temperature to form nuclei. The reactions were subsequently incubated with a range of concentrations of mitotic B1-CDK1. Nuclear envelope integrity and chromatin condensation were monitored by microscopy after

Hoechst staining (see below). The concentration (50 ng/μL) that triggered nuclear envelopment breakdown and chromosome condensation was chosen to trigger mitotic entry in subsequent experiments.

For interphase DNA replication, sperm chromatin or plasmid DNA was first incubated in HSS (final concentration of 7.5-15.0 ng DNA/μL HSS) for 30 minutes at room temperature to license the DNA for replication ("licensing"), followed by the addition of 2 volumes of NPE to initiate CDK2-dependent replication. To radiolabel the nascent strands during replication, NPE was supplemented with trace amounts of [α-³²P]-dATP. Mitotic DNA replication was performed essentially as described (Prokhorova et al., 2003). Briefly, after 30 minutes, 0.9 volumes of licensing reaction was incubated with 0.1 volumes of mitotic B1-CDK1 for 30 minutes at room temperature, followed by addition of 2 volumes of NPE. In the "licensing" mixture, the concentration of B1-CDK1 was 50 ng/μL, and its concentration in the final replication reaction was 16.7 ng/μL. Unless stated otherwise, the '0 minute' time point refers to the moment of NPE addition. 2 μL aliquots of replication reaction were stopped with 5 μL of stop solution A (5% SDS, 80 mM Tris pH8.0, 0.13% phosphoric acid, 10% Ficoll) supplemented with 1 μL 20 mg/ml Proteinase K (Roche, Nutley, NJ). Samples were incubated for 1 hour at 37°C prior to electrophoresis on a 0.9% native agarose gel. Gels were dried and radioactivity was detected using a phosphorimager (Lebofsky et al., 2009).

To induce replication fork stalling using LacR, one volume of p[lacO₄₈] (200 ng/μL) was incubated with one volume of recombinant LacR (36 μM) for 45-60 minutes at room temperature. Next, 0.1 volumes of the mixture was combined with 0.9 volumes of HSS for licensing, followed by addition of 2 volumes of NPE for initiation of replication. To inhibit the binding of LacR to the lacO array, IPTG was added to NPE to a final concentration of 10 mM and incubated for 15 minutes prior to use in replication (Figure 1E) or added into replication reactions after fork stalling (Figures S4H and S6C) at the indicated time.

For replication assays with inhibitors, NPE was supplemented with inhibitors for 15 minutes at room temperature before addition to the licensing mixture. Inhibitors were used at the following final concentrations in replication reaction: APH (Sigma Cat# A0781-5MG), 2.2 μM or 0.97 μM, as indicated; CDC7 inhibitor PHA-767491 (Sigma Cat# PZ0178), 266 μM; p97 inhibitor NMS-873 (Sigma Cat# SML1128-5MG), 266 μM; DNA-PKcs inhibitor NU-7441, 133 μM; BRC or BRC***, 1 μg/μL; Cullin inhibitor MLN-4924 (Active Biochem Cat# A-1139), 266 μM; PLK1 kinase inhibitor BI-2536 (Adooq Cat# A10134, 50 μM; Aurora A kinase inhibitor MK-5108 (Selleck Cat# S2770), 10 μM and ATR inhibitor (ETP-46464; Sigma Cat# SML1321), 200 μM. For the CDK1 inhibition assay in Figure S1G, CDK1 inhibitor RO-3306 (EMD Millipore Cat# 217699-5MG) was incubated with the replication reaction containing stalled replication forks for 5 minutes before the addition of B1-CDK1.

Immunodepletion and western blotting
Immunodepletions using antibodies against Xenopus laevis FANCD2 (Knipscheer et al., 2009), FANCI (Duxin et al., 2014), SMC2 (antigen: Ac-CSKTKERRNRMEVDK-OH, New England Peptide), TRAIP (antigen: Ac-CTSSLANQPRLEDFLK-OH, New England Peptide), Polθ (antigen: residues 1212 to 1506, Abgent), and RAD51 (Long et al., 2011) were performed as described previously (Budzowska et al., 2015). Briefly, Protein A Sepharose Fast Flow beads (GE Healthcare) were incubated with antibodies at 4°C overnight. For mock depletion, an equivalent quantity of nonspecific rabbit IgGs was used. Five volumes of pre-cleared HSS or NPE were then mixed with one volume of the antibody-bound Sepharose beads. For FANCI-D2 depletion of HSS and NPE, two rounds of depletion using both FANCI and FANCD2 antibodies were performed at room temperature for 20 minutes each. Depletions for other proteins were performed at 4°C, with two rounds for HSS and three rounds for NPE. For each round, a mixture of antibody-bound beads and egg extract was rotated on a wheel for 40 minutes. Immunodepleted extracts were collected and used immediately for DNA replication. Depletion efficiency was assessed by western blotting. Western blots from depletion or plasmid/sperm chromatin pull-downs were probed using antibodies against SMC2, TRAIP, FANCI (Duxin et al., 2014), FANCD2 (Knipscheer et al., 2009), MCM7 (Dewar et al., 2017), MCM6 (Dewar et al., 2017), RAD51 (Long et al., 2011), ORC2 (Dewar et al., 2017), CDC45 (Walter and Newport, 2000), SLD5 (Dewar et al., 2017), CHK1-pS345 (Cell Signaling Technology Cat# 2348S), γ-H2AX (Cell Signaling Technology Cat# 2577S) and Histone H3 (Cell Signaling Technology Cat# 9715S).

Sperm chromatin spin-down assay
Sperm chromatin spin-down was performed as previously described (Räschle et al., 2015). Briefly, chromatin and associated proteins were isolated by centrifugation through a sucrose cushion, washed three times, resuspended in 2x SDS sample buffer (100 mM Tris pH 6.8, 4% SDS, 0.2% bromophenol blue, 20% glycerol, 10% β-mercaptoethanol) and boiled at 95°C for 3-5 minutes. In Figure S3A, chromatin was spun down 20 minutes after NPE addition for the Buffer control and at 9 minutes after NPE addition for the B1-CDK1 treatment (final concentration, 16.7 ng/μL), at which point replication was ~50% complete for both reactions. In Figure S1D, chromatin and associated proteins were isolated from HSS.

Plasmid pull-down assay
Plasmid pull-down assays were performed as described (Budzowska et al., 2015). Briefly, streptavidin-coupled magnetic beads (Dynabeads M-280, Invitrogen; 6 μL beads slurry per pull-down) were washed three times with wash buffer 1 (50 mM Tris pH 7.5, 150 mM NaCl, 1 mM EDTA pH 8, 0.02% Tween-20). Biotinylated LacR was incubated with the beads (12 pmol per 6 μL beads) at room temperature for 40 min. The beads were then washed four times with pull-down buffer 1 (10 mM HEPES pH 7.7, 50 mM KCl, 2.5 mM MgCl2, 250 mM sucrose, 0.25 mg/mL BSA, 0.02% Tween-20) and resuspended in 40 μL of the same buffer. At the indicated times, 4 μL samples of the replication reaction were withdrawn and gently mixed with Biotin-LacR-coated beads. The

suspension was immediately placed on a rotating wheel and incubated for 30-60 minutes at 4°C. The beads were washed three times with wash buffer 2 (10 mM HEPES pH 7.7, 50 mM KCl, 2.5 mM MgCl$_2$, 0.25 mg/mL BSA, 0.03% Tween-20). The beads were resuspended in 40 μL of 2 × SDS sample buffer and boiled at 95°C for 3-5 minutes. Chromatin-bound proteins were separated by SDS-PAGE and analyzed by western blotting.

De-ubiquitination assay

Plasmid pull-downs were performed as described above, except that after the wash steps with wash buffer 2, chromatin-bound proteins were resuspended in 20 μL of USP21 buffer (150 mM NaCl, 10 mM DTT, 50mM Tris pH 7.5) and split into two 10 μL aliquots. Each aliquot was incubated with the non-specific deubiquitinase USP21 or buffer at 37°C for 60 minutes. The reactions were stopped by addition of 2x SDS sample buffer and boiled at 95°C for 3-5 minutes.

Restriction digestion

Two-microliter aliquots of replication reactions were stopped in 20 μL of stop solution B (50 mM Tris pH 7.5, 0.5% SDS, 25 mM EDTA), and replication products were purified as previously described (Räschle et al., 2008). Purified products were digested with restriction enzymes as *per* the manufacturer's instructions. Digestion reactions were stopped in 0.5 volumes of stop solution C (5% SDS, 4 mg/mL Proteinase K) and incubated for 60 minutes at room temperature. Digested products were separated on a 1% native agarose gel and visualized by autoradiography.

Sequencing

LacR-bound p[*lacO$_{48}$*] plasmid was replicated in the presence of mitotic B1-CDK1 for 120 minutes. Replication products were purified and digested with AlwNI (single cut on the parental DNA) for 60 minutes at 37°C, as described above. After separation on a 0.9% native agarose gel, bands smaller than the 4.6 kb full-length linear fragment were extracted and self-ligated with T4 DNA ligase. The ligation products were transformed into *E.coli* DH5α or XL1-Gold. As a control, p[*lacO$_{48}$*] was replicated without LacR for 120 minutes in the presence of B1-CDK1. Replication products (containing only open circular and supercoiled species) were processed as above, and the only band (4.6 kb) after AlwNI restriction was purified for cloning. Clones from both treatments were sequenced by Sanger method with Forward primer: 5′-AAGGCGATTAAGTTGGGTAA-3′ and Reverse primer: 5′-CATGTTCTTTCCTGCGTTATCCCCTGA-3′.

RNA interference

RNAi was performed by feeding worms with RNase III-deficient HT115 bacteria transformed with an L4440-derived plasmid that express double-stranded RNA (Timmons and Fire, 1998). For microscopy experiments, bacterial culture grown to OD600 = 1 was supplemented with 1 mM IPTG to express dsRNA. 400 μL of bacteria were loaded onto a 6 cm RNAi plates (3 g/L NaCl, 20 g/L agarose, 5 mg/L cholesterol, 1 mM CaCl$_2$, 1 mM MgSO$_4$, 2.7 g/L KH$_2$PO$_4$, 0.89 g/L K$_2$HPO$_4$, 1 mM IPTG and 100 mg/L Ampicillin) and the plate was incubated overnight at room temperature. For each immunoprecipitation, 0.5 mL of bacterial pre-culture grown overnight was used to inoculate a 400 mL culture in 'Terrific Broth' (12 g/L tryptone, 24 g/L yeast extract, 9.4 g/L K2HPO4, 2.2 g/L KH2PO4, adjusted to pH 7). After 7 h of growth in a baffled flask at 37°C with agitation, expression of dsRNA was induced overnight at 20°C by addition of 3 mM IPTG and the bacteria were pelleted. 8 g of bacterial pellet was resuspended with 2 mL buffer (M9 medium supplemented with 75 mg/L cholesterol; 100 mg/L ampicillin; 50 mg/L tetracycline; 12.5 mg/L amphotericin B; 3 mM IPTG) and spread on a 15 cm plate containing NGM supplemented with 1 mM IPTG and 100 mg/L ampicillin.

The plasmids expressing dsRNA were made by cloning PCR products amplified from cDNA into the vector L4440. *lrr-1* fragment was obtained with the primers ATGCGATTACCATGTGAAGTGG and CCTCGTGTGTGTATTCGATATTATC; *npl-4* fragment with GTCCAAAAGGGCCCAACTGTC and CCAGCAGGAACATCCACCAGC; *B0432.13* (*trul-1*) with ATGACGTCACAGCCCACGTCATC and CGTATTCCGTAAGATTCGACGTA. To target *lrr-1* and *B0432.13* simultaneously, DNA fragments from each gene were cloned contiguously into a single L4440 plasmid. The empty L4440 plasmid was used as control.

Microscopy

Worms at the larval L4 stage were incubated on 6 cm RNAi feeding plates for 30-34 hours at 25°C. Embryos were dissected in M9 medium (6 g/L Na$_2$HPO$_4$, 3 g/L KH$_2$PO$_4$, 5 g/L NaCl, 0.25 g/L MgSO$_4$) and mounted on a 2% agarose pad. Time lapse images were then recorded at 23–24°C using an Olympus IX81 microscope (MAG Biosystems) with a CSU-X1 spinning-disk confocal imager (Yokogawa Electric Corporation), a Cascade II camera (Photometrics) and a 60X/1.40 Plan Apochromat oil immersion lens (Olympus). Images were captured every 10 s using MetaMorph software (Molecular Devices) as previously described (Sonneville et al., 2017).

To image sperm chromatin in egg extracts, 1 μL of nuclear assembly reactions containing LSS egg extract and sperm chromatin was mixed with 1 μL of Hoechst 3300 (2.5 μg/mL) for 5 minutes before imaging. Images in Figures S1A and S1C were single focal planes acquired by a wide field Nikon Eclipse E600 microscope equipped with a Nikon 40x Plan Apo NA 1.0 oil objective. Images in Figure S4B were maximum projections from stacks of *z*-series acquired with a 0.5 μm step size. Images were collected using a 60x Plan Apo NA 1.4 oil objective with a CoolSnapHQ2 CCD camera (Photometrics) on a Yokogawa CSU-22 spinning disk confocal system (Nikon Instruments, Melville, NY). Fluorophores were excited by a 405 nm laser.

Extracts of worm embryos and immunoprecipitation of protein complexes

Preparation of worm extracts and immunoprecipitation of GFP-PSF-1 was performed as previously described (Sonneville et al., 2017). Briefly, 1 mL of a synchronized population of L4 worms expressing GFP-PSF-1 were fed for 50 h at 20°C on a 15 cm RNAi plate, supplemented with 8 g of bacterial pellet (see above). After feeding, the worms were washed in M9 medium and then disrupted in 'bleaching solution' (for 100 mL: 36.5 mL H2O, 45.5 mL 2 N NaOH and 18 mL ClNaO 4%), before washing of the resulting embryo preparation in M9 medium.

At 4°C, embryos were washed twice with lysis buffer (100 mM HEPES-KOH pH 7.9, 50 mM potassium acetate, 10 mM magnesium acetate, 2 mM EDTA), and then resuspended in three volumes of lysis buffer that was supplemented with 2 mM sodium fluoride, 2 mM sodium β-glycerophosphate pentahydrate, 1 mM dithiothreitol (DTT), 1% Protease Inhibitor Cocktail (P8215, Sigma-Aldrich), and 1 × 'Complete Protease Inhibitor Cocktail' (05056489001, Roche). The washed embryo suspension was then snap frozen drop-wise in liquid nitrogen and stored at −80°C. Subsequently, ~2.5 g of frozen embryos was ground in a SPEX SamplePrep 6780 Freezer/Mill. After thawing, we added a one-quarter volume of 'glycerol-mix' buffer (lysis buffer supplemented with 50% glycerol, 300 mM potassium acetate, 0.5% detergent IGEPAL CA-630, protease inhibitors, and DTT at the concentrations mentioned above). De-ubiquitylase enzymes were inhibited by addition of 5 μM propargylated ubiquitin (Ubi-PrG; MRC PPU, Dundee), and chromosomal DNA was digested with 1,600 U of Pierce Universal Nuclease (123991963, Fisher) for 30 min at 4°C. Extracts were centrifuged at 25,000 x g for 30 min and then for 100,000 x g for 1 h, before pre-incubation with agarose beads (0.4 mL slurry) for 45 min. Samples of each extract were taken and combined with Laemmli buffer, before storage at −80°C. The remainder was then incubated for 90 min with 40 μL of GFP-Trap_A beads (Chromotek). The beads were washed four times with 1 mL of wash buffer (100 mM HEPES-KOH pH 7.9, 100 mM potassium acetate, 10 mM magnesium acetate, 2 mM EDTA, 0.1% IGEPAL CA-630, 2 mM sodium fluoride, 2 mM sodium β-glycerophosphate pentahydrate, plus protease inhibitors as above). Finally, the bound proteins were eluted at 95°C for 5 min in 100 μl of 1 × Laemmli buffer and stored at −80°C.

Data quantification

Autoradiographs and western blots were quantified using ImageJ 1.48v (National Institute of Health). The quantification methods for individual results are described in the figure legends.